The Ubiquitin-Proteasome System Is Indispensable for the Maintenance of Muscle Stem Cells

Yasuo Kitajima,[1,2,*] Naoki Suzuki,[3] Aki Nunomiya,[4] Shion Osana,[4] Kiyoshi Yoshioka,[1] Yoshitaka Tashiro,[5] Ryosuke Takahashi,[6] Yusuke Ono,[1,*] Masashi Aoki,[3] and Ryoichi Nagatomi[4,*]

[1]Musculoskeletal Molecular Biology Research Group, Nagasaki University Graduate School of Biomedical Sciences, Basic and Translational Research Center for Hard Tissue Disease, 1-7-1 Sakamoto, Sakamoto, Nagasaki 852-8588, Japan
[2]Japan Society for the Promotion of Science, Tokyo, Japan
[3]Department of Neurology, Tohoku University School of Medicine, Sendai, Japan
[4]Division of Biomedical Engineering for Health and Welfare, Tohoku University Graduate School of Biomedical Engineering, 2-1 Seiryomachi, Aoba-ku, Sendai 980-8575, Japan
[5]Department of Aging Neurobiology, National Center for Geriatrics and Gerontology, Obu City, Japan
[6]Department of Neurology, Kyoto University Graduate School of Medicine, Kyoto, Japan
*Correspondence: yasuo.kitajima1108@gmail.com (Y.K.), yusuke-ono@nagasaki-u.ac.jp (Y.O.), nagatomi@med.tohoku.ac.jp (R.N.)
https://doi.org/10.1016/j.stemcr.2018.10.009

SUMMARY

Adult muscle stem cells (satellite cells) are required for adult skeletal muscle regeneration. A proper balance between quiescence, proliferation, and differentiation is essential for the maintenance of the satellite cell pool and their regenerative function. Although the ubiquitin-proteasome is required for most protein degradation in mammalian cells, how its dysfunction affects tissue stem cells remains unclear. Here, we investigated the function of the proteasome in satellite cells using mice lacking the crucial proteasomal component, *Rpt3*. Ablation of *Rpt3* in satellite cells decreased proteasome activity. Proteasome dysfunction in *Rpt3*-deficient satellite cells impaired their ability to proliferate, survive and differentiate, resulting in defective muscle regeneration. We found that inactivation of proteasomal activity induced proliferation defects and apoptosis in satellite cells. Mechanistically, insufficient proteasomal activity upregulated the p53 pathway, which caused cell-cycle arrest. Our findings delineate a critical function of the proteasome system in maintaining satellite cells in adult muscle.

INTRODUCTION

Adult muscle stem cells, also known as muscle satellite cells, which are the resident tissue stem cells of skeletal muscle, provide myonuclei for postnatal muscle growth and for maintenance and regeneration in adults (Blau et al., 2015; Morgan and Partridge, 2003; Relaix and Zammit, 2012; Yin et al., 2013). Satellite cells are located between the basal lamina and the plasmalemma of myofibers (Mauro, 1961). Postnatal myogenesis comprises the activation of quiescent satellite cells, the proliferation of myoblasts (activated satellite cells), and the fusion of myoblasts into multinucleated fibers. Myogenesis is a complex process that is controlled by the spatiotemporal expression of transcription factors including myogenic regulatory factors (MRFs) (Braun and Gautel, 2011; Parker et al., 2003; Wagers and Conboy, 2005).

The ubiquitin-proteasome pathway is responsible for most protein degradation in mammalian cells (Collins and Goldberg, 2017). Proteasomal degradation is mediated by the 26S proteasome, which is an ATP-dependent protease complex that is present in both the cytoplasm and nucleus. The ubiquitin-proteasome pathway has emerged as a central player in the regulation of several diverse cellular processes and functions by catalyzing the selective degradation of short-lived regulatory proteins as well as abnormal proteins. Thus, understanding the role of the proteasome in each cell and tissue type is essential for comprehending the maintenance of homeostasis.

The 26S proteasome is composed of one proteolytically active cylinder-shaped particle (the 20S proteasome) and ATPase-containing complexes (the 19S cap complexes) (Baumeister et al., 1998). The 19S cap complex unfolds ubiquitin-conjugated proteins to allow their entry into the 20S cylindrical particle. It also contains several putative ATPases, such as Rpt1–6. These subunits form a large family with a highly conserved ATPase domain (Sakao et al., 2000). Rpt3, also known as PSMC4, is an essential subunit of the 26S proteasome and is required for the degradation of most proteasomal substrates. In particular, *Rpt3*-deficient mice die before implantation due to a defect in blastocyst development (Sakao et al., 2000); this indicates that *Rpt3* is essential for survival. Interestingly, an insertion/deletion variant in intron 5 of the *Rpt3* gene was frequently found in a cohort of patients with Parkinson's disease (Marx et al., 2007). To explore the organ- and cell-specific role of the proteasome, we generated proteasome-deficient mice by targeting *Rpt3* (Kitajima et al., 2014; Tashiro et al., 2012). Previously, we found that conditional knockout of *Rpt3* in motor neurons results in locomotor dysfunction, which was accompanied by progressive motor neuron loss and gliosis in mice (Tashiro et al., 2012). Recently, we also reported that muscle-specific *Rpt3* knockout mice exhibit proteasome insufficiency, leading
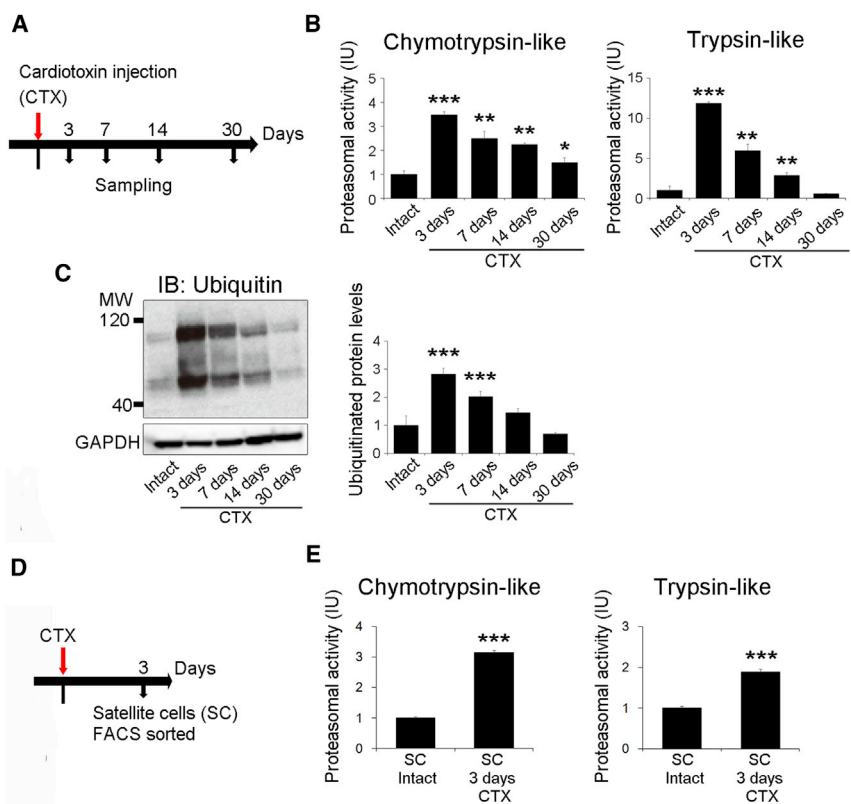
Figure 1. Proteasome Activity in Skeletal Muscle during Muscle Regeneration

(A) Time course for CTX treatment and tissue harvesting.

(B) Chymotrypsin-like and trypsin-like proteasome activities (relative to those in intact tissue) in tibialis anterior (TA) muscles at 3, 7, and 14 days after injury are shown. Data represent means ± SEM (t test: *p < 0.05, **p < 0.01, ***p < 0.001 versus intact; n = 3–5 per group). IU, international units.

(C) Immunoblotting analysis of ubiquitin in the TA muscles at 3, 7, and 14 days post injury. Data represent means ± SEM (t test: ***p < 0.001 versus intact; n = 3–5 per group).

(D) Time course analysis of satellite cells at 3 days after injury.

(E) Chymotrypsin-like and trypsin-like proteasome activities (relative to those in intact satellite cells) in satellite cells sorted from TA muscles at 3 days post injury. Data represent means ± SEM (t test: ***p < 0.001 versus intact satellite cells; n = 4–5 per group). IU, international units.

See also Figures S1.

to obvious muscle atrophy (Kitajima et al., 2014). Furthermore, centrally nucleated regenerating fibers were observed in muscle-specific *Rpt3* knockout mice, indicating the involvement in muscle regeneration. However, it remains unclear how the proteasome system regulates satellite cells. Here, we investigated the pathophysiological effect of proteasome insufficiency induced by depletion of *Rpt3* on satellite cells *in vivo* and *in vitro* by using satellite cell-specific *Rpt3*-knockout mice.

RESULTS

Proteasome Activity in Skeletal Muscle during Muscle Regeneration

As the first step to determine proteasome activity in muscle during skeletal muscle regeneration, we induced skeletal muscle injury by injecting cardiotoxin (CTX) into the tibialis anterior (TA) muscle in mice. First, we analyzed the regenerative capacity of C57BL/6J mice over time (Figure S1A). On days 14 and 30 after injury, the weight of CTX-injected muscles was significantly increased compared with that of intact muscles (Figure S1B). At 30 days post injury, the mean TA muscle weight per body weight was also increased compared with that of intact muscle (Figure S1C). Furthermore, histo-

logical analysis revealed extensive muscle damage and the infiltration of inflammatory cells into the muscle at 3 days post CTX injection, whereas centrally nucleated regenerating fibers began to be visible at day 7 post injury (Figure S1D). Following muscle injury, satellite cells start to express *MyoD* and become myoblasts (PAX7+/MYOD + cells) to proliferate (Yin et al., 2013). Quantitative PCR (qPCR) analysis confirmed that mRNA levels of *MyoD*, *Pax7*, and *Myh3*, markers of regenerating fibers, peaked at day 3 post injury (Figure S1E).

We next examined the proteasome system during regeneration after CTX-induced muscle injury. The ubiquitin-proteasome system degrades most long- and short-lived normal and abnormal intracellular proteins (Collins and Goldberg, 2017; Goldberg, 2003). We used lysates from regenerating muscle tissue to evaluate chymotrypsin-like and trypsin-like proteasome activities during muscle regeneration. Chymotrypsin-like and trypsin-like proteasome activities drastically increased to a peak level at 3 days post injury, progressively declined until day 14, and then returned to levels comparable to those observed in uninjured control tissues by 30 post injury (Figures 1A and 1B). Because most proteasomal substrates must be ubiquitinated before degradation (Schrader et al., 2009), we analyzed ubiquitinated proteins during muscle regeneration by

immunoblotting. Consistent with the proteasomal activities, we showed that the amount of ubiquitinated proteins increased, peaking at 3 days after injury and then returning to basal levels by 30 days post injury (Figure 1C). Because chymotrypsin-like and trypsin-like proteasome activity dramatically increased to a peak level 3 days after injury (Figure 1B), we then examined proteasome activity in only myocytes, excluding non-muscle cells, such as inflammatory cells, on day 3 post injury. At this time point, chymotrypsin-like and trypsin-like proteasome activities were significantly higher in myoblasts from injured animals, compared with those from control mice (Figures 1D, 1E, S1F, and S1G). These results showed that proteasome activity is dramatically increased in skeletal muscle and myoblasts during the early phase of muscle regeneration.

Satellite Cell-specific *Rpt3*-Knockout Mice Exhibit No Obvious Phenotype in Muscle

To investigate the function of the proteasome system in satellite cells, we generated satellite cell-specific *Rpt3* conditional knockout (*Rpt3*-scKO) mice by crossing *Pax7^CreERT2* mice (Lepper and Fan, 2010) with *Rpt3^f/f* mice (Kitajima et al., 2014; Tashiro et al., 2012). Previously, we reported that deficiency of *Rpt3* in skeletal muscle or motor neurons causes proteasome insufficiency (Kitajima et al., 2014; Tashiro et al., 2012). First, we examined the expression levels of *Rpt3* in muscle stem cells during proliferation and differentiation. Upon activation, muscle satellite cells proliferate, downregulate *Pax7*, and differentiate (Kitajima and Ono, 2018; Yin et al., 2013). *Rpt3* gene expression in satellite cell-derived myoblasts did not differ during the proliferation and differentiation processes (Figure S2). Genetic inactivation of *Rpt3* was induced by repeated intraperitoneal injection of tamoxifen (Tmx) into adult *Pax7^CreERT2/+*; *Rpt3^f/f* mice, using Tmx-treated *Rpt3^f/f* littermates as the wildtype control (Figure 2A). Following Tmx treatment *in vivo*, *Rpt3* expression was significantly reduced in satellite cells (Figure 2B). In addition, chymotrypsin-like and trypsin-like proteasome activities were significantly lower in satellite cells from *Rpt3*-scKO mice (Figure 2C). Moreover, *Rpt3* gene knockdown was performed in the C2C12 myoblast cell line (Figure S3A). Two small interfering RNAs (siRNAs) were used and siRNA (#2) resulted in a greater than 90% reduction in *Rpt3* expression (Figure S3B), and thus was used in further experiments. Evaluation of proteasome function revealed that chymotrypsin-like and trypsin-like protease activities were significantly decreased 48 and 72 hr after gene knockdown (Figure S3C). These results revealed the efficiency of the satellite cell-specific *Rpt3* conditional knockout in our mouse model.

Next, we investigated the effect of *Rpt3* deficiency in satellite cells on skeletal muscle *in vivo*. There was no change in body weight between control and *Rpt3*-scKO mice

from 1 to 8 months after Tmx treatment (Figure 2D). There was also no difference in TA muscle weight (Figure 2E) and H&E staining of muscle cross sections (Figure 2F) 2 months after Tmx treatment. Other than limb muscles, in the diaphragm, there was no difference in the H&E staining of muscle cross sections and muscle cross-sectional area, 1 month after Tmx treatment (Figures S4A–S4C). Furthermore, when we performed an endurance test to investigate muscle function, there was no significant difference between control and *Rpt3*-scKO mice (Figure 2G). These results suggest that satellite cell-specific *Rpt3* knockout has no obvious effect on intact muscle in mice.

Satellite Cell-specific *Rpt3*-scKO Mice Are Associated with a Remarkable Defect in Regeneration

To evaluate the role of *Rpt3* in satellite cells during muscle regeneration *in vivo*, we genetically inactivated *Rpt3* via five daily intraperitoneal injections of Tmx into *Pax7^CreERT2/+*; *Rpt3^f/f* mice. Intramuscular injection of CTX was performed to induce regeneration of the TA muscle after 2 days of Tmx treatment (Figure 3A). We showed the muscle weight was markedly decreased in *Rpt3*-scKO mice after regeneration compared with that in control mice at day 7 and 14 post CTX treatment (Figures 3B–3D). Correspondingly, histological analysis confirmed a significant defect in muscle regeneration accompanied by a considerable number of infiltrating inflammatory cells in *Rpt3*-scKO mice at day 14 after CTX treatment, although efficient muscle regeneration accompanied by centrally nucleated myofibers was observed in control mice (Figure 3E). Immunohistochemistry also revealed incomplete regeneration with marked fibrosis at day 14 post CTX treatment in *Rpt3*-scKO mice (Figure 3F). In addition, the cross-sectional area of the regenerated fibers was decreased at day 14 post CTX treatment in *Rpt3*-scKO mice (Figure 3G). To evaluate muscle regeneration in the early phase, we assessed the expression of MYOD, which is a marker of myoblasts. MYOD+ cells were not frequently found in *Rpt3*-scKO mice 3 days after CTX treatment (Figure 3H). Taken together, our data indicate that the function of *Rpt3* in satellite cell is indispensable for muscle regeneration *in vivo*.

Loss of *Rpt3* Leads to a Depletion of the Quiescent Satellite Cell Pool

Previous studies have confirmed the absolute necessity of PAX7-positive satellite cells for muscle regeneration (Lepper et al., 2011; Relaix and Zammit, 2012; Sambasivan et al., 2011; von Maltzahn et al., 2013). Because muscle regeneration was impaired in *Rpt3*-scKO mice, we next examined how *Rpt3* knockout affects quiescent satellite cells in adult resting skeletal muscles. After 5 consecutive days of Tmx injection, we found a surprisingly rapid decline in the number of quiescent satellite cells in freshly
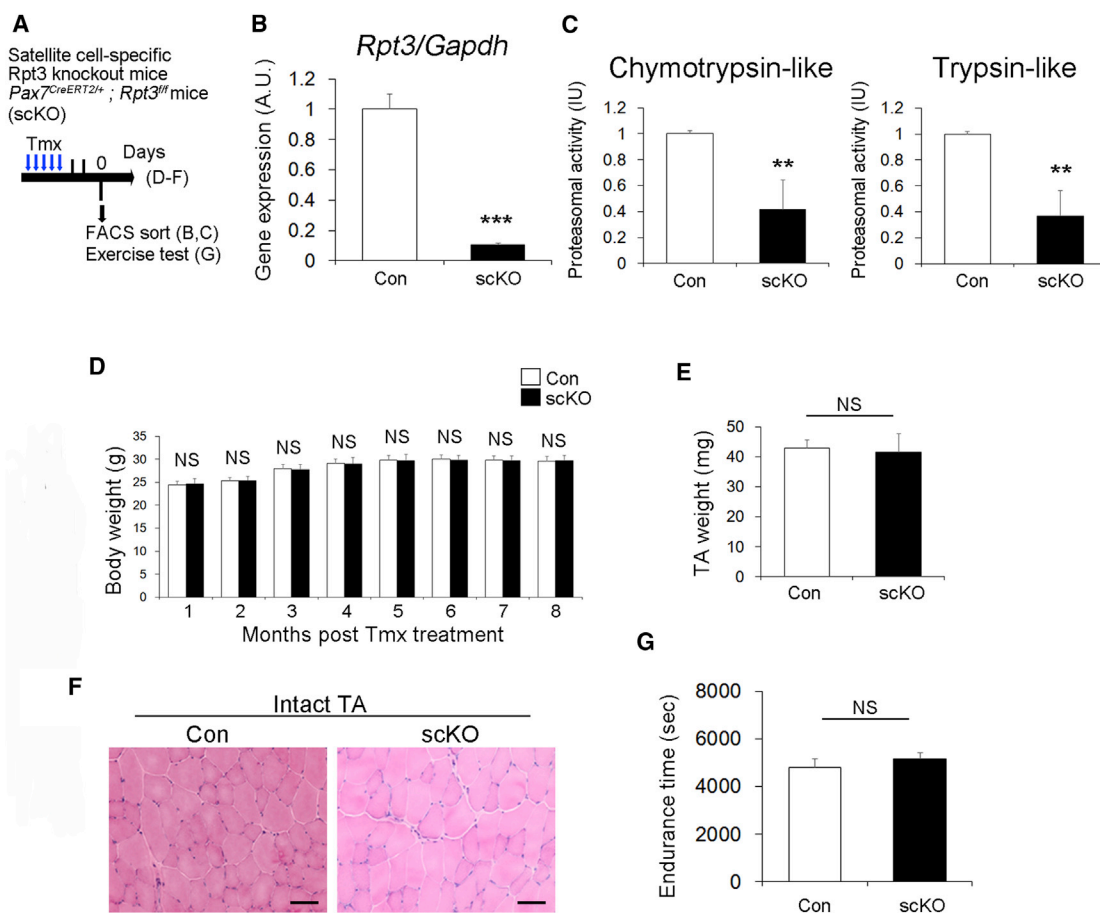
Figure 2. Satellite Cell-specific *Rpt3*-Knockout Mice Exhibit No Obvious Skeletal Muscle Phenotype

(A) Time course for tamoxifen (Tmx) treatment and tissue harvesting. Con indicates *Rpt3^{f/f}* mice and scKO indicates satellite cell-specific *Rpt3*-knockout mice (*Pax7^{CreERT2/+}; Rpt3^{f/f}*).

(B) Relative expression of *Rpt3* mRNA in freshly isolated satellite cells derived from Con and scKO mice after Tmx injection. Data represent means ± SEM (t test: ***p < 0.001; n = 4 per group). AU, arbitrary units.

(C) Chymotrypsin-like and trypsin-like proteasome activities (relative to Con) in freshly isolated satellite cells derived from Con and scKO mice after Tmx injection. Data represent means ± SEM (t test: **p < 0.01; n = 4–5 per group). IU, international units.

(D) Change in body weight (g) after Tmx injection. Data represent mean ± SD (NS, statistically nonsignificant, n = 5–10 per group).

(E) Change in tibialis anterior (TA) muscle weight (g) at 2 months after Tmx injection. Data represent mean ± SD (NS, statistically nonsignificant, n = 4–6 per group).
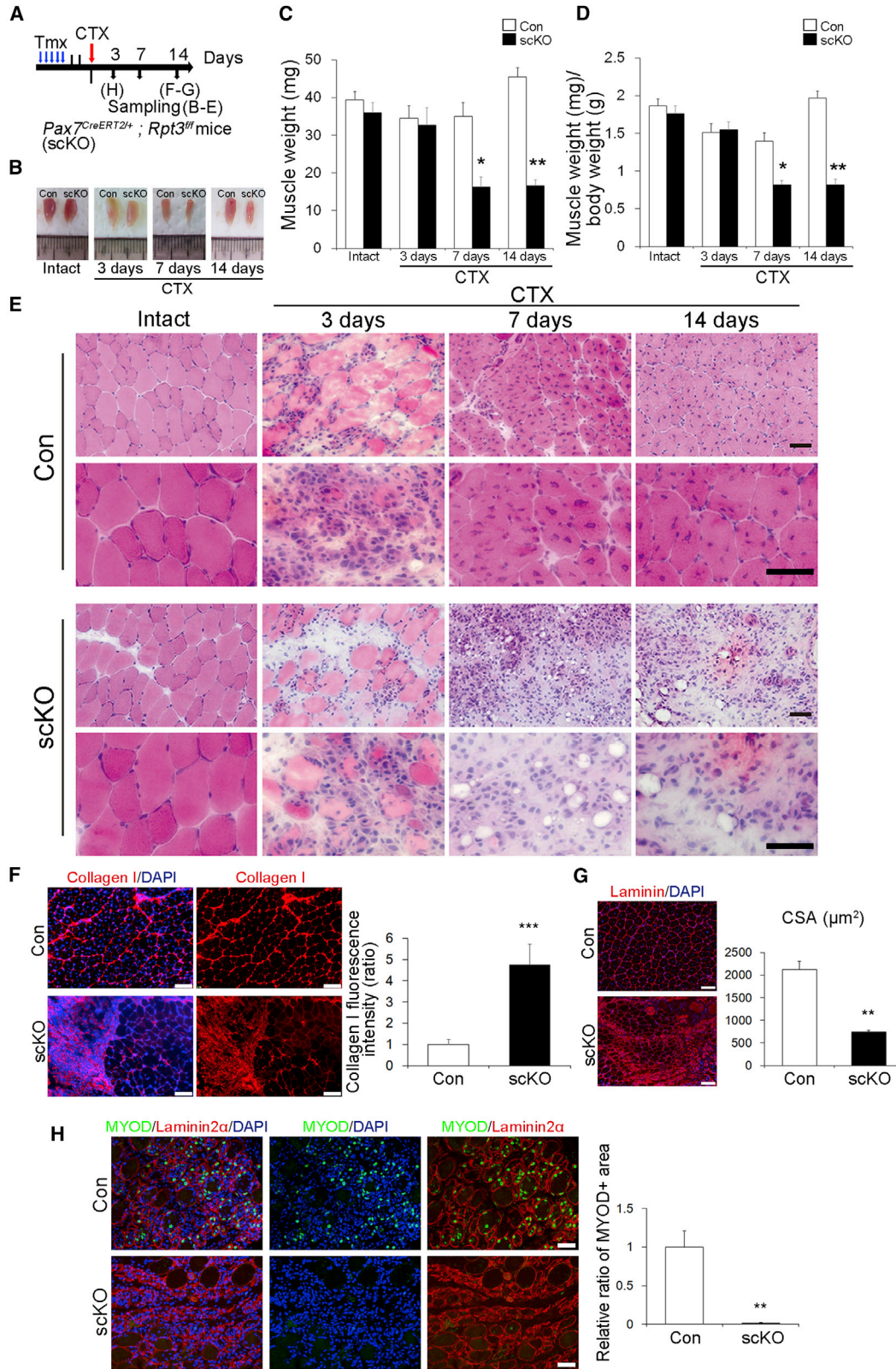
(F) H&E staining of intact TA muscle 2 months after Tmx injection. Scale bar, 50 μm. Also shown in Figure S1D.

(G) Endurance time(s) of Con and scKO mice. Data represent mean ± SD (NS, statistically nonsignificant, n = 4–6 per group).

See also Figures S2–S4.

isolated extensor digitorum longus (EDL) myofibers from *Rpt3*-scKO mice, but not in those from control mice (Figures 4A–4C). Specifically, 20% of quiescent satellite cells were lost within 5 days, 80% were lost within 10 days, and 90% were lost within 15 days in *Rpt3*-scKO mice (Figure 4C). Similarly, immunofluorescence staining for PAX7 and laminin in TA muscle cross sections indicated the robust ablation (90% loss) of PAX7+ quiescent satellite cells in *Rpt3*-scKO mice at day 15 after Tmx treatment (Figures 4D and 4E). In addition, immunofluorescence staining

for M-cadherin, as another satellite cell marker in TA and diaphragm muscles, revealed a robust decrease in satellite cells in *Rpt3*-scKO mice (Figures 4F, 4G, S4D, and S4E). We further analyzed the number of quiescent satellite cells in limb muscles by flow cytometry. We confirmed the rapid depletion of the satellite cell fraction in *Rpt3*-scKO mice, consistent with immunohistochemical analysis (Figures 4H, 4I, and S5A–S5D). These results demonstrate that loss of *Rpt3* leads to depletion of quiescent satellite cells in adult resting muscle.

A

Tmx CTX
|||| ↓   3 7 14 Days
      (H)   (F-G)
      Sampling (B-E)
Pax7^CreERT2/+ ; Rpt3^f/f mice
(scKO)

B

Con scKO   Con scKO   Con scKO   Con scKO

Intact   3 days   7 days   14 days
                      CTX

C

□ Con
■ scKO

Muscle weight (mg)

Intact   3 days   7 days   14 days
                  CTX

* **

D

□ Con
■ scKO

Muscle weight (mg)/body weight (g)

Intact   3 days   7 days   14 days
                  CTX

* **

E

Intact   CTX
          3 days   7 days   14 days

Con

scKO

F

Collagen I/DAPI   Collagen I

Con

scKO

Collagen I fluorescence intensity (ratio)

Con   scKO

***

G

Laminin/DAPI

Con

scKO

CSA (µm²)

Con   scKO

**

H

MYOD/Laminin2α/DAPI   MYOD/DAPI   MYOD/Laminin2α

Con

scKO

Relative ratio of MYOD+ area

Con   scKO

**

(legend on next page)

Deficiency of *Rpt3* in Satellite Cells Results in Proliferative Defects during Muscle Regeneration *In Vivo*

To clarify whether the loss of satellite cells in *Rpt3*-scKO mice is caused by apoptosis, we performed apoptosis experiments using Cleaved-Caspase 3 *in vivo* (Figure 5A). Numbers of Cleaved-Caspase 3+ cells relative to PAX7+ cells were significantly increased in the intact TA muscle of *Rpt3*-scKO mice, 3 days after Tmx treatment (Figure 5B). Next, to elucidate cell proliferation in the satellite cells of *Rpt3*-scKO mice *in vivo*, we performed EdU incorporation assays and immunostaining for KI67, a proliferative marker that is not expressed in G0 cells (Figure 5C). The proliferative ability of intact TA muscle in *Rpt3*-scKO mice was not different from that in control mice (Figures 5D and 5E).

Moreover, to examine the proliferative potential of *Rpt3*-scKO satellite cells during muscle regeneration, an EdU incorporation assay was performed (Figure 5F). EdU+ M-cadherin+ cells were significantly decreased in *Rpt3*-scKO mice when compared with the control mice (Figure 5G). These data suggested that the deficiency of *Rpt3* in satellite cells results in proliferative defects during muscle regeneration *in vivo*.

Deletion of *Rpt3* in Satellite Cells Induces a Proliferation Defect and Apoptosis

We next focused on how the proliferative state of satellite cells is affected by proteasome dysfunction mediated by *Rpt3*-deficiency *in vitro*. Satellite cells isolated from *Pax7^CreERT2/+*; *Rpt3^f/f* mice were plated and treated with 4-hydroxy tamoxifen (4OH-Tmx) for 2 days to genetically delete *Rpt3* in satellite cells (Figure 6A). Expression of *Rpt3* was suppressed by 85% in *Rpt3* KO satellite-cell-derived myoblasts compared with that in control myoblasts (Figure 6B). Cell proliferation was evaluated by performing EdU incorporation assays *in vitro*. The proliferative ability of *Rpt3*-deficient primary myoblasts was decreased compared with that in controls (Figure 6C). In addition, to investigate whether cell proliferation defects also occur

after *Rpt3* knockdown in other cells, *Rpt3*-knockdown experiments were performed using primary fibroblasts (Figure S6A). Cell proliferation was suppressed in primary fibroblasts with *Rpt3*-knockdown compared with that in controls (Figures S6B and S6C).

We next asked if *Rpt3*-knockout-satellite cells can undergo myogenic differentiation. Two days after the induction of differentiation, control myoblasts already displayed an obviously elongated morphology, a hallmark of differentiation (Figures S7A and S7B). In contrast, *Rpt3*-scKO primary myoblasts were mostly spherical (Figure S7B), indicative of a differentiation defect. We further quantified the differentiation index, which measures the fraction of myonuclei that are located in myosin heavy chain (MyHC+)-expressing cells. Although greater than 50% of nuclei in the control were located in MyHC+ cells, only 15% of nuclei in *Rpt3*-scKO mice were found in MyHC+ cells (Figure S7B).

To determine if the reduction in satellite cell-derived myoblasts proliferation was also due to cell death, apoptosis was evaluated by performing TUNEL assays. TUNEL-positive apoptotic cells were detected more frequently in primary myoblasts of *Rpt3*-scKO mice (Figure 6D). This was further supported by the upregulation of Cleaved-Caspase 3, an indicator of apoptosis, in *Rpt3*-inactivated primary myoblasts (Figure 6E). Consistent with these results, the number of cells was reduced in *Rpt3*-scKO mice compared with that in control mice (Figure 6F). Upon knockdown of *Rpt3*, proliferation and cell numbers decreased, whereas apoptotic cells were more frequently detected in *Rpt3*-ablated cells (Figures 6G–6J). These results demonstrate that proteasome dysfunction mediated by *Rpt3* deficiency in satellite cells induces a proliferation defect and apoptosis.

p53 Knockdown in *Rpt3*-Deficient Satellite Cells Rescues the Defect in Proliferation

We next investigated the molecular mechanism underlying *Rpt3* deficiency-induced dysfunction in activated satellite cells. To identify the pathways affected by *Rpt3*

Figure 3. Satellite Cell-specific Deletion of *Rpt3* Prevents Muscle Regeneration

(A) Time course for tamoxifen (Tmx) and cardiotoxin (CTX) treatment. Con indicates *Rpt3^f/f* mice and scKO indicates satellite cell-specific *Rpt3* knockout mice (*Pax7^CreERT2/+*; *Rpt3^f/f*).

(B) Representative images of tibialis anterior (TA) muscles in Con and scKO mice.

(C and D) Change in (C) muscle weight (mg) and (D) muscle weight (mg)/body weight (g). Data represent mean ± SEM (t test: *p < 0.05, **p < 0.01 versus Con, n = 5–9 per group).

(E) H&E staining of intact muscles and those injured by CTX injection, analyzed at 3, 7, and 14 days post injury. Scale bar, 50 μm.

(F) Immunostaining of collagen I (red) and DAPI (blue) in TA muscle cryosections from scKO mice 14 days after injury. Scale bar, 100 μm. The y axis shows the mean collagen I fluorescence intensity (ratio). Data represent means ± SEM (t test: ***p < 0.001; n = 5 per group).

(G) Immunostaining of Laminin (red) and DAPI (blue) in TA muscle cryosections from scKO mice 14 days after injury. Scale bar, 100 μm. The y axis shows the mean cross-sectional area (CSA). Data represent means ± SD (t test: **p < 0.01; n = 3 per group).

(H) Immunostaining for MYOD (green), Laminin2α, and DAPI (blue) in TA muscle cryosections from scKO mice 3 days after injury. Scale bar, 50 μm. The y axis shows the relative ratio of MYOD-positive areas. Data represent means ± SD (t test: **p < 0.01; n = 3 per group).
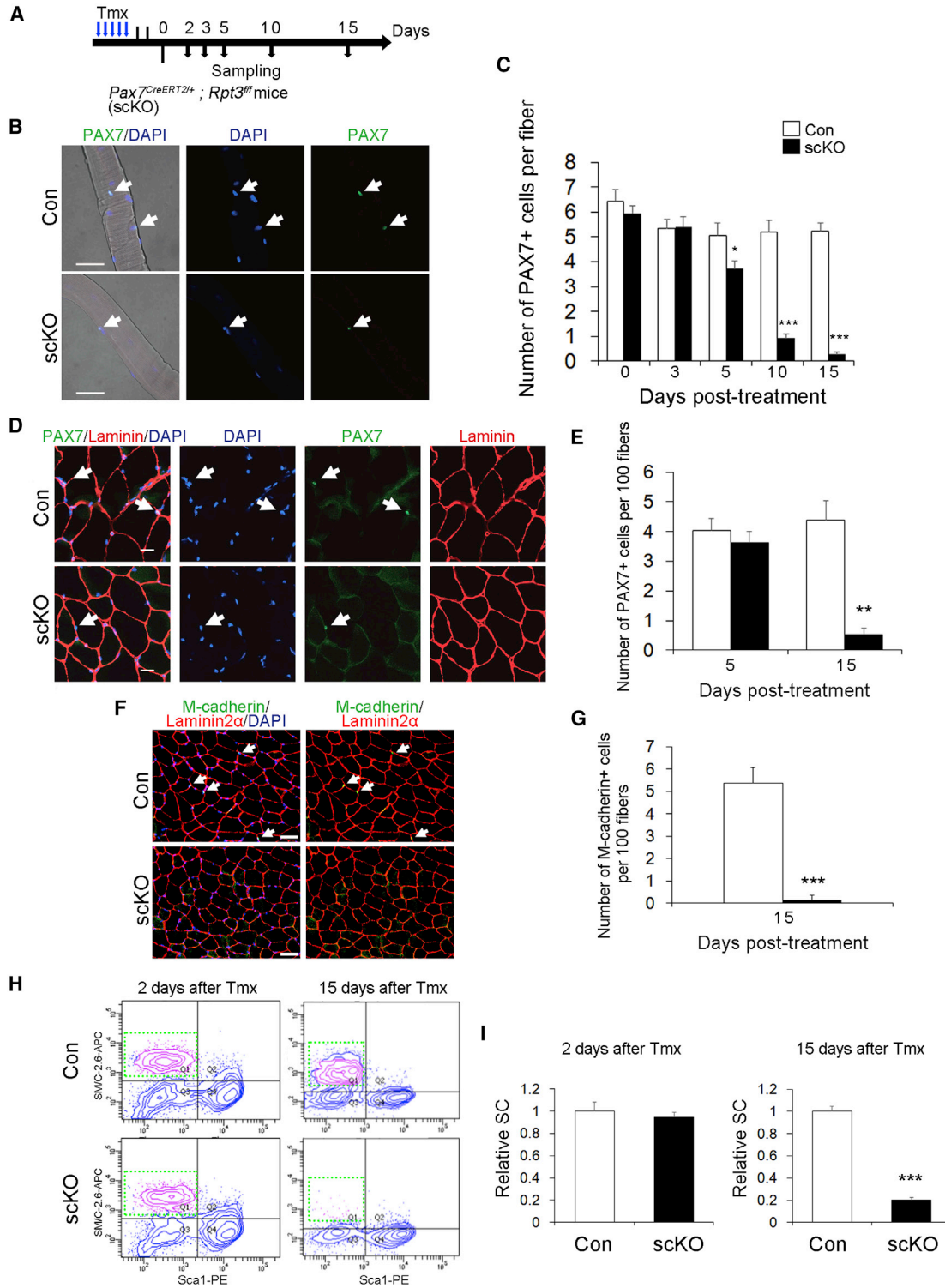
Figure 4. Rpt3 Inactivation Depletes the Satellite Cell Pool

(A) Time course of tamoxifen (Tmx) treatment and tissue harvesting. Con indicates *Rpt3^{f/f}* mice and scKO indicates satellite cell-specific *Rpt3* knockout mice (*Pax7^{CreERT2/+}; Rpt3^{f/f}*).

(B) Immunostaining for PAX7 (green) and DAPI (blue) in the extensor digitorum longus (EDL) single fiber 5 days after Tmx induction. Arrows indicate satellite cells. Scale bar, 50 μm.

(legend continued on next page)

deficiency in an unbiased manner, we performed microarray analysis of quiescent satellite cells from control and *Rpt3*-scKO mice (accession number GSE114354). We identified 1,254 genes that were up- or downregulated with p values < 0.05 (Table S2). Significantly differentially expressed genes were imported into the DAVID v6.7 annotation tool, and Kyoto Encyclopedia of Genes and Genomes (KEGG) pathway analysis was performed. The enrichment of specific pathway components into functionally regulated gene groups was characterized with reference to the KEGG pathway database. This analysis identified the top two categories as being related to the proteasome and p53 signaling pathways (Figure 7A).

p53 is known to inhibit cell proliferation by both blocking cell-cycle progression and promoting apoptotic cell death (Vousden and Prives, 2009). As shown in Figures 6C, 6D, 6H, and 6I, suppression of cell proliferation and induction of apoptotic cell death was observed in *Rpt3*-scKO mice. We therefore examined whether the p53 pathway is involved in the regulation of *Rpt3*-scKO satellite cells. Satellite cells isolated from *Pax7^{CreERT2/+}*; *Rpt3^{f/f}* mice were plated and then treated with 4OH-Tmx for 2 days to genetically delete *Rpt3* in satellite cells (Figure 7B). Expression of *Rpt3* was suppressed by 80% in *Rpt3* KO satellite-cell-derived myoblasts compared with that in control myoblasts (Figure 7C). As expected, levels of *p53*, as well as *p21*, which is a well-known p53-downstream target, were elevated, whereas *Cyclind1* and *Cdk4*, which are cell-cycle-related genes associated with *p53*, were suppressed in *Rpt3*-scKO satellite cell-derived myoblasts (Figure 7C). Consistent with mRNA levels, western blotting also demonstrated a dramatic increase in p53 protein and its phosphorylation (ser392) in *Rpt3*-scKO satellite cell-derived myoblasts (Figure 7D). p53-related proliferation is regulated by phosphorylated Rb, which was decreased in *Rpt3*-scKO satellite cell-derived myoblasts (Figure 7D). Moreover, based on immunohistochemistry, a greater than 20-fold increase in the number of p53-positive cells was confirmed in *Rpt3*

KO satellite-cell-derived myoblasts as compared with those in controls (Figure 7E). These results demonstrate that *Rpt3* deletion in satellite-cell-derived myoblasts leads to the activation of p53 signaling in satellite cells.

Finally, to test if activation of p53 signaling is responsible for the inhibition of proliferation in *Rpt3*-scKO mice, we examined the effect of p53 silencing on *Rpt3*-null satellite cell-derived myoblasts. p53 knockdown was performed in C2C12 cells (Figure S7C). Two siRNAs were used and siRNA (#2) showed greater than 90% reduction in *p53* gene expression (Figures S7D–S7F) and was thus used for further experiments. Satellite cells isolated from *Pax7^{CreERT2/+}*; *Rpt3^{f/f}* mice were plated and then treated with 4OH-Tmx for 2 days after *p53* siRNA transfection (Figure 7F). Importantly, the proliferative ability as well as the number of cells were both restored in *Rpt3*-null myoblasts when transfected with *p53* siRNA (Figures 7G, 7H, S7G, and S7I), although the differentiation ability was not improved with *p53* knockdown (Figures S7J and S7K). Taken together, these results show that knockdown of *p53* rescues defective proliferation in *Rpt3*-deficient primary myoblasts.

DISCUSSION

In this study, we report that the proteasome system is indispensable for the maintenance of muscle stem cells. Ablation of *Rpt3* in satellite cells impairs their ability to proliferate, survive, and differentiate, resulting in a severe defect in muscle regeneration. We also found that proteasome inactivation by *Rpt3* deficiency in primary myoblasts inhibits cell proliferation and induces apoptosis. Further, proteasome dysfunction conferred by satellite cell-specific *Rpt3* knockout induces p53 activation. Previously, it was determined that p53 inhibits cell proliferation by both blocking cell-cycle progression and promoting apoptotic cell death (Vousden and Prives, 2009). We also found that p53 knockdown rescued cell proliferation defects in *Rpt3*-deficient myoblasts.

(C) Number of satellite cells per fresh EDL myofiber from Con and scKO mice 0–15 days after Tmx treatment. Data represent mean ± SEM (t test: *p < 0.05, ***p < 0.001; day 0, n = 5; day 3, n = 4; day 5, n = 5; day 10, n = 5; day 15, n = 4 per group; more than 15 myofibers per animal).

(D) Immunostaining for PAX7 (green), laminin (red), and DAPI (blue) in tibialis anterior (TA) muscle cryosections 5 days after Tmx treatment. Arrows indicate satellite cells. Scale bar, 20 μm.

(E) Average number of satellite cells per 100 fibers. Data represent mean ± SEM (t test: **p < 0.01; day 5, n = 4; day 15, n = 5 for each group).

(F) Immunostaining for M-cadherin (green), Laminin2α (red), and DAPI (blue) in intact TA muscle cryosections from scKO mice. Arrows indicate satellite cells. Scale bar, 50 μm.

(G) Average number of M-cadherin+ cells per 100 fibers. Data represent means ± SD (t test: ***p < 0.001; n = 3 per group).

(H) Fluorescence-activated cell sorting profiles of mononuclear cells derived from Con and scKO mice 2 and 15 days after Tmx treatment. The gated profiles show satellite cell fractions (SM/C-2.6 + CD31− CD45− Sca1−) from Con and scKO mice.

(I) Relative satellite cell fractions from Con and scKO mice. Data represent mean ± SEM (t test: ***p < 0.001; day 2, n = 4; day 15, n = 4 per group). SC, satellite cell.
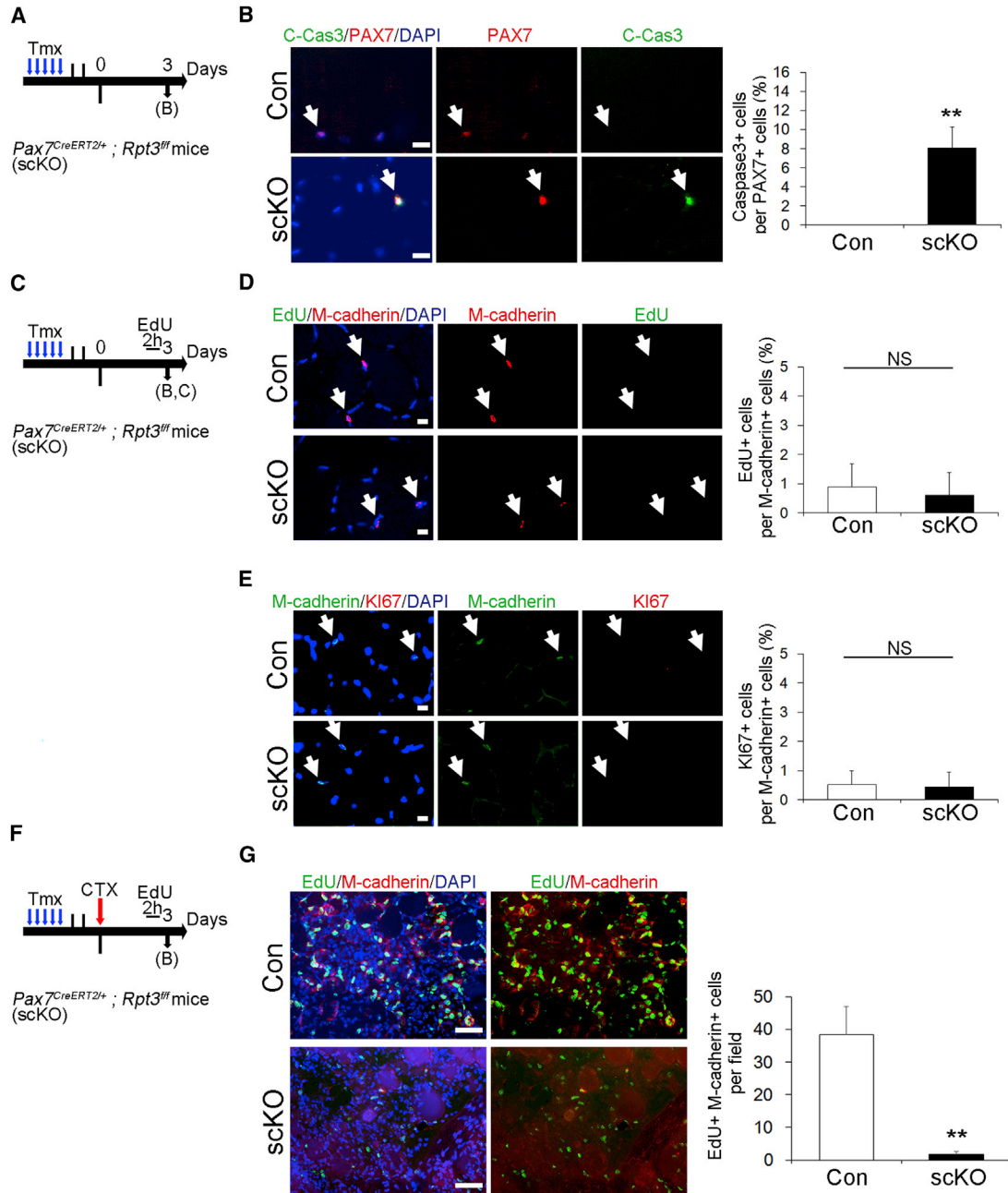
See also Figures S4 and S5.

Figure 5. Deficiency of *Rpt3* in Satellite Cells Results in Proliferative Defects during Muscle Regeneration *In Vivo*

(A) Time course for tamoxifen (Tmx) treatment and tissue harvesting. Con indicates *Rpt3^{f/f}* mice and scKO indicates satellite cell-specific *Rpt3* knockout mice (*Pax7^{CreERT2/+}*; *Rpt3^{f/f}*).

(B) Immunostaining for Cleaved-Caspase3 (green), Pax7 (red), and DAPI (blue) in tibialis anterior (TA) muscle cryosections 3 days after Tmx treatment. Arrows indicate satellite cells. Scale bar, 10 μm. The y axis shows the ratio of Cleaved-Caspase3-positive cells to PAX7-positive cells. Data represent means ± SD (t test: **p < 0.01; n = 3 per group).

(C) Time course for Tmx treatment and tissue harvesting.

(D) Immunostaining for EdU (green), M-cadherin (red), and DAPI (blue) in TA muscle cryosections, 3 days after Tmx treatment. Arrows indicate satellite cells. Scale bar, 10 μm. The y axis shows the ratio of EdU-positive cells to M-cadherin-positive cells. Data represent means ± SD (t test: NS, no significance; n = 3 per group).

(legend continued on next page)

The ubiquitin-proteasome system functions to degrade most long- and short-lived normal and abnormal intracellular proteins (Collins and Goldberg, 2017; Goldberg, 2003). Especially in muscle, proteolysis by the ubiquitin-proteasome system is a major mechanism involved in myofibrillar protein degradation (Attaix et al., 1998; Hasselgren et al., 2002). Therefore, when examining proteasome activity during regeneration, we found that both chymotrypsin-like and trypsin-like proteasome activities were increased 3 days after CTX injection, indicating that the early phase of muscle regeneration is associated with the activation of machinery involved in protein degradation. Furthermore, the accumulation of ubiquitinated proteins was also most accelerated on day 3 post injury, indicating that proteasome-related proteolysis was most enhanced at this time point. Interestingly, MYOD, which constitutes an important myogenic transcription factor for muscle regeneration (Charge and Rudnicki, 2004; Sabourin et al., 1999), was also particularly elevated on day 3 post injury. In a previous study, proteasome activity was found to be strongly correlated with proliferating cell nuclear antigen protein levels, suggesting that the proteasome plays a key role in myoblast proliferation (Duguez et al., 2003). Thus, it is suggested that enhancing the proteasome system during the early phase is an important event for normal muscle regeneration.

Previous studies have confirmed the absolute requirement for Pax7-positive satellite cells during muscle regeneration (Lepper et al., 2011; Relaix and Zammit, 2012; Sambasivan et al., 2011; von Maltzahn et al., 2013). Our data support these findings that satellite cells are essential for muscle regeneration. When the number of satellite cells decreases, muscle regeneration fails. These data might indicate that the number of satellite cells is also important. However, other cells. such as mesoangioblasts and PW1+ interstitial cells, which contribute to regeneration, have been identified in muscle tissue (Mitchell et al., 2010; Sampaolesi et al., 2003). Thus, we cannot exclude the possibility that the regenerative defect in Rpt3-scKO mice at day 14 after CTX injection could be improved after a long period of recovery by contributing to the myogenic potential of other cells involved in regeneration (Mitchell et al., 2010; Sampaolesi et al., 2003).

Proteasome insufficiency due to Rpt3 deficiency increased the protein levels of Cleaved-Caspase 3 and caused apoptosis. Furthermore, we performed immunoblotting analysis of Bax, Bak, Bcl-2, and Mcl-1 proteins related to apoptosis, but there was no significant change particularly (data not shown). A previous study reported that the proteasome inhibitor MG132 induces caspase-3-dependent apoptosis, and a caspase-3 inhibitor was found to reduce MG132-induced apoptosis in human mast cells (Westerberg et al., 2012). Our data show that proteasome dysfunction by loss of Rpt3 is accompanied by apoptosis, which is at least due to enhancement of the caspase 3 activity. Therefore, in this study, it is considered that apoptosis in scKO primary myoblasts might be alleviated by the inhibition of Caspase 3.

There have been many previous studies on the association between the proteasome system and p53. Among these, one report suggested that the ubiquitination level of p53 is elevated after treatment with the proteasome inhibitor MG132 (Maki et al., 1996), suggesting that this protein is degraded by the proteasome and that its stability is controlled by ubiquitin-dependent degradation. Consistent with these findings, we demonstrated p53 stability in primary myoblasts exhibiting proteasome dysfunction (via Rpt3 ablation). p53 inhibits cell proliferation by both blocking cell-cycle progression and promoting apoptotic cell death (Vousden and Prives, 2009). In addition, proteasome inhibition has been shown to induce apoptosis in several different cell types (Concannon et al., 2007; Ding et al., 2007; Pandit and Gartel, 2011). Therefore, we hypothesized that proteasome dysfunction, mediated by Rpt3 deletion, results in cell death and the inhibition of cell proliferation due to p53 hyperactivation. Because p53 is upregulated in Rpt3-deficient myoblasts, we examined whether knockdown of p53 rescues the proliferation defects observed in Rpt3-deficient myoblasts. Importantly, we found that inhibition of p53 successfully rescued these effects, indicating that the proteasome system in muscle stem cells regulates cell proliferation at least in part through p53.

Myogenesis is a complex process controlled by the spatiotemporal expression of many MRFs and transcription factors (Braun and Gautel, 2011; Parker et al., 2003; Wagers and Conboy, 2005). As myoblast differentiation proceeds, the timely synthesis and degradation of

(E) Immunostaining for M-cadherin (green), KI67 (red), and DAPI (blue) in TA muscle cryosections, 3 days after Tmx treatment. Arrows indicate satellite cells. Scale bar, 10 μm. The y axis shows the ratio of KI67-positive cells to M-cadherin-positive cells. Data represent means ± SD (t test: NS, no significance; n = 3 per group).
(F) Time course for Tmx treatment and tissue harvesting.
(G) Immunostaining for EdU (green), M-cadherin (red), and DAPI (blue) in TA muscle cryosections, 3 days after injury. Scale bar, 50 μm. The y axis shows the number of EdU-positive and M-cadherin-positive cells per field. Data represent means ± SD (t test: **p < 0.01; n = 3 per group).
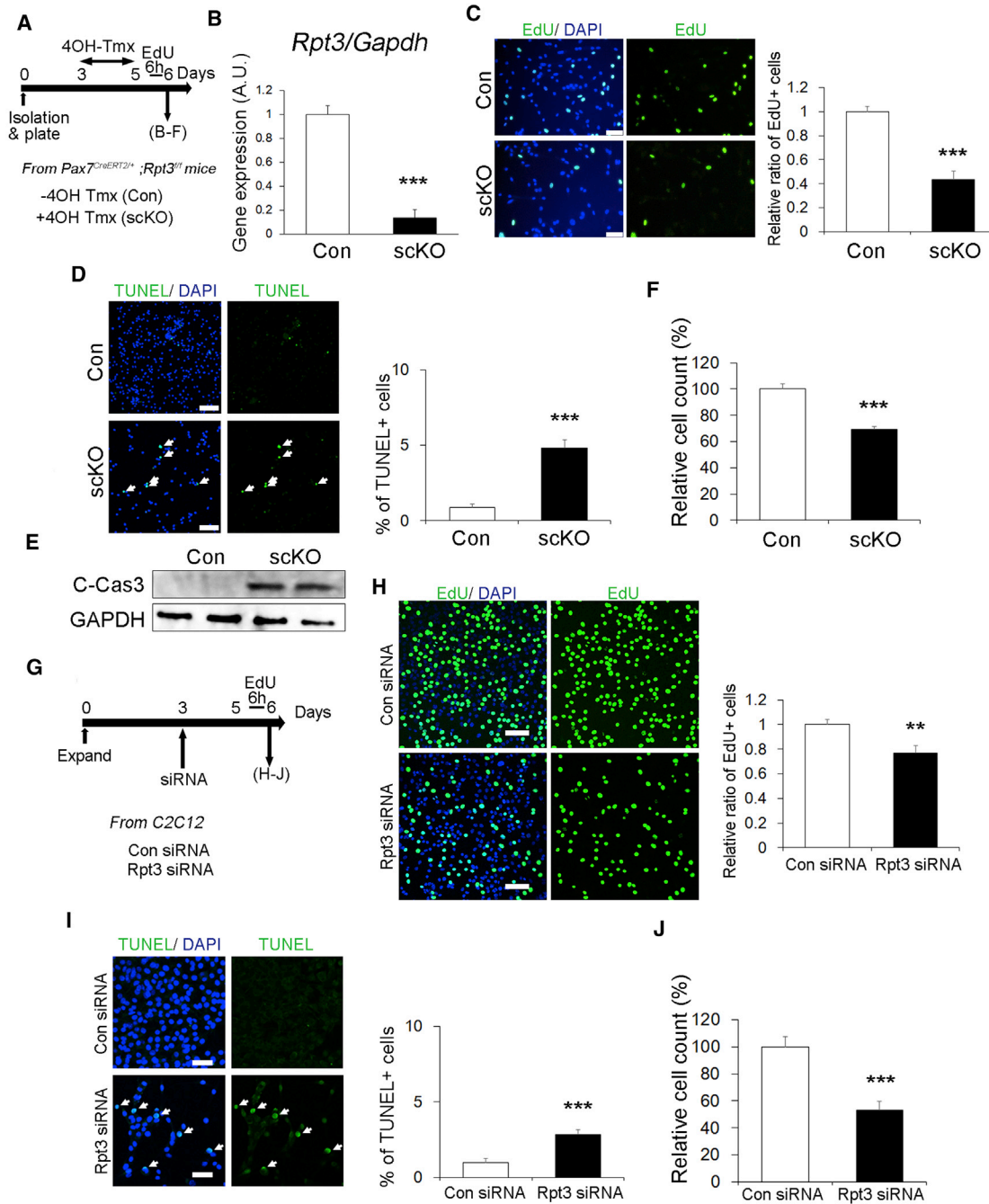
Figure 6. Deletion of *Rpt3* in Satellite Cells Induces a Proliferation Defect and Apoptosis

(A) Time course for tamoxifen (Tmx) treatment and tissue harvesting. Con indicates *Rpt3*$^{f/f}$ mice and scKO indicates satellite cell-specific *Rpt3* knockout mice (*Pax7*$^{CreERT2/+}$; *Rpt3*$^{f/f}$).

(B) Relative expression of *Rpt3* mRNA in *Pax7*$^{CreERT2/+}$; *Rpt3*$^{f/f}$ satellite cells treated with vehicle or 4OH-Tmx. Data represent means ± SEM (t test: ***p < 0.001; n = 3 per group). AU, arbitrary units.

(C) Immunostaining for EdU (green) and DAPI (blue) in satellite cells treated with vehicle or 4OH-Tmx. Scale bar, 50 μm. The y axis shows the relative ratio of EdU-positive cells. Data represent means ± SEM (t test: ***p < 0.001; n = 4 per group).

(D) Immunostaining for TUNEL (green) and DAPI (blue) in satellite cells treated with vehicle or 4OH-Tmx. Arrows indicate TUNEL-positive cells. Scale bar, 100 μm. The y axis shows the ratio of TUNEL-positive cells to DAPI-positive cells. Data represent means ± SEM (t test: ***p < 0.001; n = 3 per group).

(legend continued on next page)

appropriate myogenic proteins are required, which suggests a significant role for adaptive proteolysis in the myogenic process. Indeed, previous studies have reported that the complex process of myogenic differentiation, which begins with cell-cycle arrest and ends with the fusion of individual myoblasts to form multinucleated myotubes, is related to the proteasome system (Abu Hatoum et al., 1998; Gardrat et al., 1997; Kim et al., 1998). In addition, inhibition or knockdown of the proteasome can block the fusion of myoblasts and inhibit differentiation (Gardrat et al., 1997; Kim et al., 1998). Consistent with previous studies, proteasome dysfunction conferred by Rpt3 deficiency was found to suppress the myogenic differentiation of primary myoblasts, suggesting that proper proteasome function is necessary for myogenic differentiation. In addition, it has been previously shown that p53 can promote muscle differentiation in vitro (Halevy et al., 1995; Porrello et al., 2000; Soddu et al., 1996; Tamir and Bengal, 1998; Weintraub et al., 1991). However, despite the presence of p53 observed in Rpt3-deficient primary myoblasts, Rpt3 ablation was shown to suppress myogenic differentiation. This might be because p53 expression was excessive. Indeed, a 20-fold increase in p53-positive cells was observed in Rpt3-deficient myoblasts, as compared with that in controls, based on immunostaining. A recent study reported that tight control of p53 levels in myoblasts regulates the balance between differentiation and return to quiescence (Flamini et al., 2018), which could indicate appropriate expression of p53 during myogenic differentiation.

Satellite cells provide myonuclei for postnatal muscle growth and for maintenance and regeneration in adults (Relaix and Zammit, 2012; Yin et al., 2013), indicating that the maintenance of satellite cells is essential for the functional homeostasis of skeletal muscle. Moreover, recent studies indicated that skeletal muscle disease is exacerbated by defective satellite cells (Crist, 2017). Importantly, we found that proteasome dysfunction by loss of Rpt3 in satellite cells leads to a dramatic depletion of the quiescent satellite cell pool approximately 2 weeks after knockout induction. Previous studies demonstrated that proteolysis by the proteasome is essential to maintain amino acid pools (Suraweera et al., 2012; Vabulas and Hartl, 2005). Although quiescent satellite cells are thought to be associated with very low turnover in steady state conditions (Lepper and Fan, 2010), minimal amino acid pools obtained from proteolysis by the proteasome system are necessary for the normal maintenance of cells. Therefore, proteasome dysfunction, conferred by Rpt3 deficiency, might have resulted in serious consequences, depriving the cells of pooled resources for cellular maintenance. We hypothesize that satellite cell-specific Rpt3 deficiency might have blocked the cellular "recycling system" that is essential for the maintenance of satellite cells; this question needs to be further examined.

Rpt3 deficiency in primary myoblasts and Rpt3 knockdown in a myoblast cell line resulted in a decrease in proteasome activity, leading to apoptotic cell death. There are several reports showing the relationship between proteasomal activity and aging, including lifespan. During aging, proteasomal activity is decreased in several tissues, such as the brain (Zeng et al., 2005), liver (Dasuri et al., 2009; Hayashi and Goto, 1998), heart (Bulteau et al., 2002), and muscle (Ferrington et al., 2005). Overexpression of proteasome subunits in yeast and Caenorhabditis elegans has been shown to lead to an increase in proteasome activity as well as prolonged lifespan (Chen et al., 2006; Vilchez et al., 2012), whereas flies and mice with a genetic decrease in proteasome activity have a shortened lifespan (Tomaru et al., 2012; Tonoki et al., 2009). Previously, we have also reported a shortened lifespan even in muscle-specific Rpt3-knockout mice (Kitajima et al., 2014). Taken together, these data suggest that there is a close relationship between the proteasome system and aging in vivo and in vitro. Whether adult somatic stem cells also have enhanced proteasome activity remains to be elucidated, but the maintenance of this activity might critically affect organismal aging (Vilchez et al., 2014). Therefore, our findings using muscle stem cells will lead to a detailed understanding of proteolysis and its associated molecular mechanisms in muscle stem cells. Our results show that the ubiquitin-proteasome system is

(E) Immunoblotting analysis of Cleaved-Caspase3 and GAPDH in satellite cells treated with vehicle or 4OH-Tmx.

(F) Relative ratio of DAPI-positive cells from Con or scKO mice. Data represent means ± SEM (t test: ***p < 0.001; n = 3 per group).

(G) Time course of Tmx treatment and tissue harvesting. Con siRNA indicates control siRNA transfection and Rpt3 siRNA indicates Rpt3 siRNA transfection.

(H) Immunostaining for EdU (green) and DAPI (blue) in C2C12 cells after siRNA transfection. Scale bar, 50 μm. The y axis shows the relative ratio of EdU-positive cells. Data represent means ± SEM (t test: **p < 0.01; n = 3 per group).

(I) Immunostaining for TUNEL (green) and DAPI (blue) in C2C12 cells after siRNA transfection. Arrows indicate TUNEL-positive cells. Scale bar, 100 μm. The y axis shows the ratio of TUNEL-positive cells to DAPI-positive cells. Data represent means ± SEM (t test: ***p < 0.001; n = 3 per group).

(J) Relative ratio of DAPI-positive cells. Data represent means ± SEM (t test: ***p < 0.001; n = 3 per group).
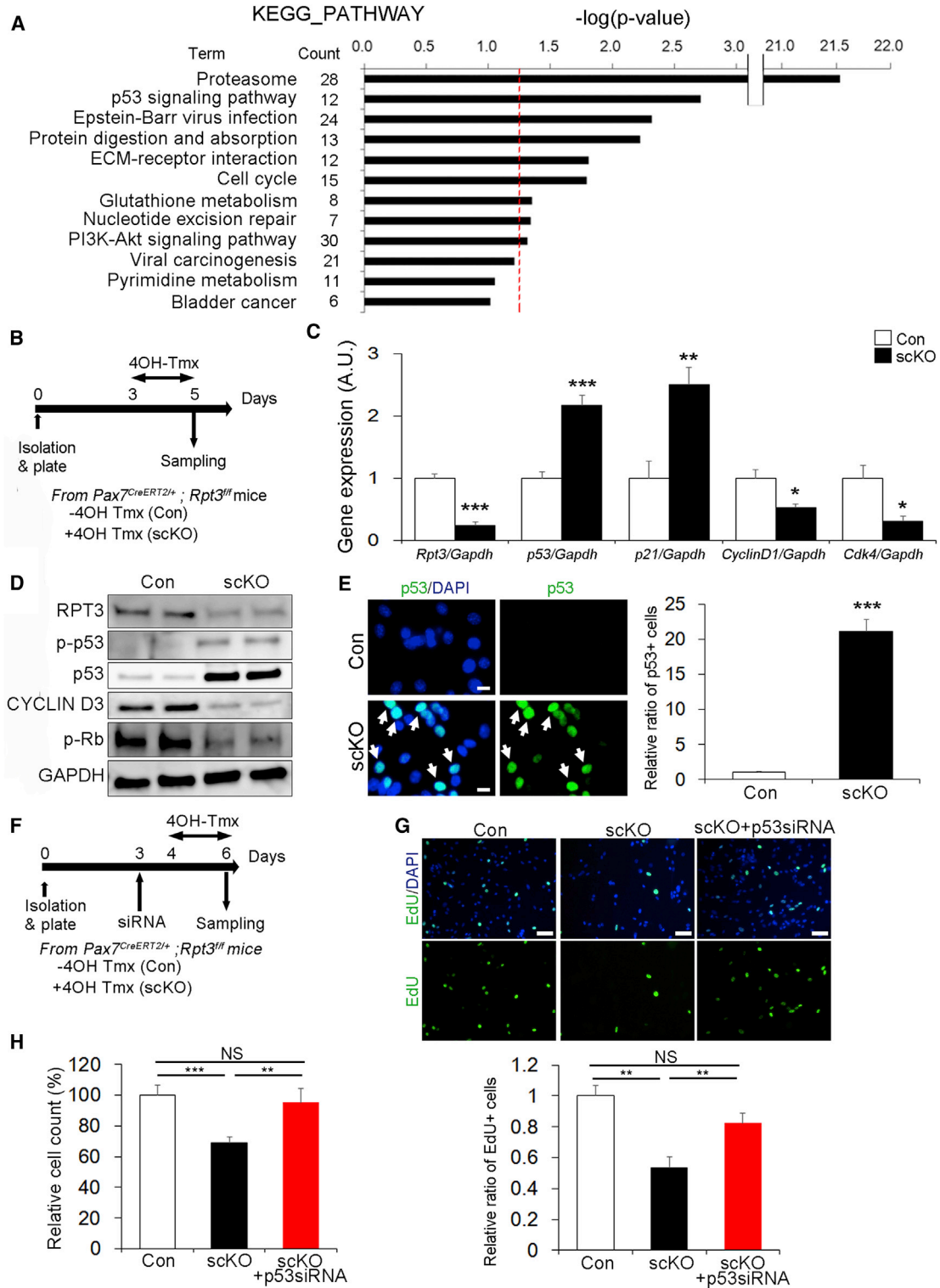
See also Figures S6 and S7.

Figure 7. p53 Knockdown in *Rpt3*-Deficient Satellite Cells Rescues the Defect in Proliferation

(A) DAVID v6.7 functional annotation bioinformatics microarray analysis software was used to obtain KEGG pathway functional classification. Only KEGG pathway terms for classification that showed statistically significant differences, in terms of the number of differentially regulated genes (satellite cells from satellite cell-specific *Rpt3* mice versus satellite cells from control mice), are shown

(legend continued on next page)

indispensable for the maintenance of muscle stem cells. Further study is needed to understand the role of stem cells in various physiological processes involving the proteasome system; however, this work provides the fundamentals for understanding the regulation of proteolysis in muscle stem cells.

EXPERIMENTAL PROCEDURES

Cell Culture

Satellite cells were cultured in GM (DMEM supplemented with 30% fetal bovine serum, 1% chick embryo extract, 10 ng/mL basic fibroblast growth factor , and 1% penicillin-streptomycin) on culture dishes coated with Matrigel (BD Biosciences). Myogenic differentiation was induced in DM (DMEM supplemented with 5% horse serum and 1% penicillin-streptomycin). For *in vitro* genetic deletion, 4-OH Tmx (1 μM) was added to culture medium for 2 days to induce Cre-mediated deletion.

Mouse C2C12 myoblasts were cultured in GM (DMEM supplemented with 10% fetal bovine serum and 1% penicillin-streptomycin). The cells were transfected with 30 nM siRNA using Lipofectamine RNAiMAX (Invitrogen).

Single Fiber Isolation

Individual myofibers were isolated from the EDL muscle as we described previously (Kitajima et al., 2016; Ono et al., 2015). In brief, EDL myofibers were digested using 0.2% type I collagenase (Worthington) in DMEM for 90 min at 37°C with 5% CO_2. Muscles were mechanically dissociated and then washed five times to eliminate debris and contaminating cells. For immunohistochemical analysis, EDL myofibers were immediately fixed using 4% paraformaldehyde (PFA, Wako) in PBS.

ACCESSION NUMBERS

The microarray dataset in this study is available from the GEO public depository under the accession number: GEO: GSE114354.

REFERENCES

Abu Hatoum, O., Gross-Mesilaty, S., Breitschopf, K., Hoffman, A., Gonen, H., Ciechanover, A., and Bengal, E. (1998). Degradation of myogenic transcription factor MyoD by the ubiquitin pathway

(p < 0.05). The 1,254 significantly differentially regulated genes are shown in Table S2. The red dash line denotes the significance level of 0.05.

(B) Time course of tamoxifen (Tmx) treatment and tissue harvesting. Con indicates $Rpt3^{f/f}$ mice and scKO indicates satellite cell-specific $Rpt3$ knockout mice ($Pax7^{CreERT2/+}$; $Rpt3^{f/f}$).

(C) Real-time RT-PCR was used to measure the mRNA expression of p53-related genes (*p53*, *p21*, *Cyclin D1*, and *Cdk4*) in $Pax7^{CreERT2/+}$; $Rpt3^{f/f}$ satellite cells treated with vehicle or 4OH-Tmx. Data represent means ± SEM (t test: *p < 0.05, **p < 0.01, ***p < 0.001; n = 4–5 per group). AU, arbitrary units.

(D) Immunoblotting analysis of relative protein levels of p53 targets in $Pax7^{CreERT2/+}$; $Rpt3^{f/f}$ satellite cells treated with vehicle or 4OH-Tmx.

(E) Immunostaining for p53 (green) and DAPI (blue) in $Pax7^{CreERT2/+}$; $Rpt3^{f/f}$ satellite cells treated with vehicle or 4OH-Tmx. Arrows indicate p53-positive cells. Scale bar, 10 μm. The y axis shows the relative ratio of p53-positive cells. Data represent means ± SEM (t test: ***p < 0.001; n = 4 per group).

(F) Time course analysis of *p53* siRNA knockdown and Tmx treatment.

(G) Immunostaining for EdU (green) and DAPI (blue) in satellite cells treated with vehicle or 4OH-Tmx. Scale bar, 50 μm. The y axis shows the relative ratio of EdU-positive cells. Data represent means ± SEM (one-way ANOVA followed by the Bonferroni post hoc test: **p < 0.01; NS, no significance; n = 4 per group).

(H) Relative ratio of DAPI-positive cells. Data represent means ± SEM (one-way ANOVA followed by the Bonferroni post hoc test: **p < 0.01, ***p < 0.01; NS, no significance; n = 4–6 per group).

See also Figure S7.

in vivo and in vitro: regulation by specific DNA binding. Mol. Cell. Biol. *18*, 5670–5677.

Attaix, D., Aurousseau, E., Combaret, L., Kee, A., Larbaud, D., Ralliere, C., Souweine, B., Taillandier, D., and Tilignac, T. (1998). Ubiquitin-proteasome-dependent proteolysis in skeletal muscle. Reprod. Nutr. Dev. *38*, 153–165.

Baumeister, W., Walz, J., Zuhl, F., and Seemuller, E. (1998). The proteasome: paradigm of a self-compartmentalizing protease. Cell *92*, 367–380.

Blau, H.M., Cosgrove, B.D., and Ho, A.T. (2015). The central role of muscle stem cells in regenerative failure with aging. Nat. Med. *21*, 854–862.

Braun, T., and Gautel, M. (2011). Transcriptional mechanisms regulating skeletal muscle differentiation, growth and homeostasis. Nat. Rev. Mol. Cell Biol. *12*, 349–361.

Bulteau, A.L., Szweda, L.I., and Friguet, B. (2002). Age-dependent declines in proteasome activity in the heart. Arch. Biochem. Biophys. *397*, 298–304.

Charge, S.B., and Rudnicki, M.A. (2004). Cellular and molecular regulation of muscle regeneration. Physiol. Rev. *84*, 209–238.

Chen, Q., Thorpe, J., Dohmen, J.R., Li, F., and Keller, J.N. (2006). Ump1 extends yeast lifespan and enhances viability during oxidative stress: central role for the proteasome? Free Radic. Biol. Med. *40*, 120–126.

Collins, G.A., and Goldberg, A.L. (2017). The logic of the 26S proteasome. Cell *169*, 792–806.

Concannon, C.G., Koehler, B.F., Reimertz, C., Murphy, B.M., Bonner, C., Thurow, N., Ward, M.W., Villunger, A., Strasser, A., Kogel, D., et al. (2007). Apoptosis induced by proteasome inhibition in cancer cells: predominant role of the p53/PUMA pathway. Oncogene *26*, 1681–1692.

Crist, C. (2017). Emerging new tools to study and treat muscle pathologies: genetics and molecular mechanisms underlying skeletal muscle development, regeneration, and disease. J. Pathol. *241*, 264–272.

Dasuri, K., Nguyen, A., Zhang, L., Fernandez-Kim, O.S., Bruce-Keller, A.J., Blalock, B.A., Cabo, R.D., and Keller, J.N. (2009). Comparison of rat liver and brain proteasomes for oxidative stress-induced inactivation: influence of ageing and dietary restriction. Free Radic. Res. *43*, 28–36.

Ding, W.X., Ni, H.M., Chen, X., Yu, J., Zhang, L., and Yin, X.M. (2007). A coordinated action of Bax, PUMA, and p53 promotes MG132-induced mitochondria activation and apoptosis in colon cancer cells. Mol. Cancer Ther. *6*, 1062–1069.

Duguez, S., Bihan, M.C., Gouttefangeas, D., Feasson, L., and Freyssenet, D. (2003). Myogenic and nonmyogenic cells differentially express proteinases, Hsc/Hsp70, and BAG-1 during skeletal muscle regeneration. Am. J. Physiol. Endocrinol. Metab. *285*, E206–E215.

Ferrington, D.A., Husom, A.D., and Thompson, L.V. (2005). Altered proteasome structure, function, and oxidation in aged muscle. FASEB J. *19*, 644–646.

Flamini, V., Ghadiali, R.S., Antczak, P., Rothwell, A., Turnbull, J.E., and Pisconti, A. (2018). The satellite cell niche regulates the balance between myoblast differentiation and self-renewal via p53. Stem Cell Reports *10*, 970–983.

Gardrat, F., Montel, V., Raymond, J., and Azanza, J.L. (1997). Proteasome and myogenesis. Mol. Biol. Rep. *24*, 77–81.

Goldberg, A.L. (2003). Protein degradation and protection against misfolded or damaged proteins. Nature *426*, 895–899.

Halevy, O., Novitch, B.G., Spicer, D.B., Skapek, S.X., Rhee, J., Hannon, G.J., Beach, D., and Lassar, A.B. (1995). Correlation of terminal cell cycle arrest of skeletal muscle with induction of p21 by MyoD. Science *267*, 1018–1021.

Hasselgren, P.O., Wray, C., and Mammen, J. (2002). Molecular regulation of muscle cachexia: it may be more than the proteasome. Biochem. Biophys. Res. Commun. *290*, 1–10.

Hayashi, T., and Goto, S. (1998). Age-related changes in the 20S and 26S proteasome activities in the liver of male F344 rats. Mech. Ageing Dev. *102*, 55–66.

Kim, S.S., Rhee, S., Lee, K.H., Kim, J.H., Kim, H.S., Kang, M.S., and Chung, C.H. (1998). Inhibitors of the proteasome block the myogenic differentiation of rat L6 myoblasts. FEBS Lett. *433*, 47–50.

Kitajima, Y., Ogawa, S., and Ono, Y. (2016). Visualizing the functional heterogeneity of muscle stem cells. Methods Mol. Biol. *1516*, 183–193.

Kitajima, Y., and Ono, Y. (2018). Visualization of PAX7 protein dynamics in muscle satellite cells in a YFP knock-in-mouse line. Skelet. Muscle *8*, 26.

Kitajima, Y., Tashiro, Y., Suzuki, N., Warita, H., Kato, M., Tateyama, M., Ando, R., Izumi, R., Yamazaki, M., Abe, M., et al. (2014). Proteasome dysfunction induces muscle growth defects and protein aggregation. J. Cell Sci. *127*, 5204–5217.

Lepper, C., and Fan, C.M. (2010). Inducible lineage tracing of Pax7-descendant cells reveals embryonic origin of adult satellite cells. Genesis *48*, 424–436.

Lepper, C., Partridge, T.A., and Fan, C.M. (2011). An absolute requirement for Pax7-positive satellite cells in acute injury-induced skeletal muscle regeneration. Development *138*, 3639–3646.

Maki, C.G., Huibregtse, J.M., and Howley, P.M. (1996). In vivo ubiquitination and proteasome-mediated degradation of p53(1). Cancer Res. *56*, 2649–2654.

Marx, F.P., Soehn, A.S., Berg, D., Melle, C., Schiesling, C., Lang, M., Kautzmann, S., Strauss, K.M., Franck, T., Engelender, S., et al. (2007). The proteasomal subunit S6 ATPase is a novel synphilin-1 interacting protein–implications for Parkinson's disease. FASEB J. *21*, 1759–1767.

Mauro, A. (1961). Satellite cell of skeletal muscle fibers. J. Biophys. Biochem. Cytol. *9*, 493–495.

Mitchell, K.J., Pannerec, A., Cadot, B., Parlakian, A., Besson, V., Gomes, E.R., Marazzi, G., and Sassoon, D.A. (2010). Identification and characterization of a non-satellite cell muscle resident progenitor during postnatal development. Nat. Cell Biol. *12*, 257–266.

Morgan, J.E., and Partridge, T.A. (2003). Muscle satellite cells. Int. J. Biochem. Cell Biol. *35*, 1151–1156.

Ono, Y., Urata, Y., Goto, S., Nakagawa, S., Humbert, P.O., Li, T.S., and Zammit, P.S. (2015). Muscle stem cell fate is controlled by the cell-polarity protein Scrib. Cell Rep. *10*, 1135–1148.

Pandit, B., and Gartel, A.L. (2011). Proteasome inhibitors induce p53-independent apoptosis in human cancer cells. Am. J. Pathol. *178*, 355–360.

Parker, M.H., Seale, P., and Rudnicki, M.A. (2003). Looking back to the embryo: defining transcriptional networks in adult myogenesis. Nat. Rev. Genet. *4*, 497–507.

Porrello, A., Cerone, M.A., Coen, S., Gurtner, A., Fontemaggi, G., Cimino, L., Piaggio, G., Sacchi, A., and Soddu, S. (2000). p53 regulates myogenesis by triggering the differentiation activity of pRb. J. Cell Biol. *151*, 1295–1304.

Relaix, F., and Zammit, P.S. (2012). Satellite cells are essential for skeletal muscle regeneration: the cell on the edge returns centre stage. Development *139*, 2845–2856.

Sabourin, L.A., Girgis-Gabardo, A., Seale, P., Asakura, A., and Rudnicki, M.A. (1999). Reduced differentiation potential of primary MyoD-/- myogenic cells derived from adult skeletal muscle. J. Cell Biol. *144*, 631–643.

Sakao, Y., Kawai, T., Takeuchi, O., Copeland, N.G., Gilbert, D.J., Jenkins, N.A., Takeda, K., and Akira, S. (2000). Mouse proteasomal ATPases Psmc3 and Psmc4: genomic organization and gene targeting. Genomics *67*, 1–7.

Sambasivan, R., Yao, R., Kissenpfennig, A., Van Wittenberghe, L., Paldi, A., Gayraud-Morel, B., Guenou, H., Malissen, B., Tajbakhsh, S., and Galy, A. (2011). Pax7-expressing satellite cells are indispensable for adult skeletal muscle regeneration. Development *138*, 3647–3656.

Sampaolesi, M., Torrente, Y., Innocenzi, A., Tonlorenzi, R., D'Antona, G., Pellegrino, M.A., Barresi, R., Bresolin, N., De Angelis, M.G., Campbell, K.P., et al. (2003). Cell therapy of alpha-sarcoglycan null dystrophic mice through intra-arterial delivery of mesoangioblasts. Science *301*, 487–492.

Schrader, E.K., Harstad, K.G., and Matouschek, A. (2009). Targeting proteins for degradation. Nat. Chem. Biol. *5*, 815–822.

Soddu, S., Blandino, G., Scardigli, R., Coen, S., Marchetti, A., Rizzo, M.G., Bossi, G., Cimino, L., Crescenzi, M., and Sacchi, A. (1996). Interference with p53 protein inhibits hematopoietic and muscle differentiation. J. Cell Biol. *134*, 193–204.

Suraweera, A., Munch, C., Hanssum, A., and Bertolotti, A. (2012). Failure of amino acid homeostasis causes cell death following proteasome inhibition. Mol. Cell. *48*, 242–253.

Tamir, Y., and Bengal, E. (1998). p53 protein is activated during muscle differentiation and participates with MyoD in the transcription of muscle creatine kinase gene. Oncogene *17*, 347–356.

Tashiro, Y., Urushitani, M., Inoue, H., Koike, M., Uchiyama, Y., Komatsu, M., Tanaka, K., Yamazaki, M., Abe, M., Misawa, H., et al. (2012). Motor neuron-specific disruption of proteasomes, but not autophagy, replicates amyotrophic lateral sclerosis. J. Biol. Chem. *287*, 42984–42994.

Tomaru, U., Takahashi, S., Ishizu, A., Miyatake, Y., Gohda, A., Suzuki, S., Ono, A., Ohara, J., Baba, T., Murata, S., et al. (2012). Decreased proteasomal activity causes age-related phenotypes and promotes the development of metabolic abnormalities. Am. J. Pathol. *180*, 963–972.

Tonoki, A., Kuranaga, E., Tomioka, T., Hamazaki, J., Murata, S., Tanaka, K., and Miura, M. (2009). Genetic evidence linking age-dependent attenuation of the 26S proteasome with the aging process. Mol. Cell. Biol. *29*, 1095–1106.

Vabulas, R.M., and Hartl, F.U. (2005). Protein synthesis upon acute nutrient restriction relies on proteasome function. Science *310*, 1960–1963.

Vilchez, D., Morantte, I., Liu, Z., Douglas, P.M., Merkwirth, C., Rodrigues, A.P., Manning, G., and Dillin, A. (2012). RPN-6 determines C. elegans longevity under proteotoxic stress conditions. Nature *489*, 263–268.

Vilchez, D., Simic, M.S., and Dillin, A. (2014). Proteostasis and aging of stem cells. Trends Cell Biol. *24*, 161–170.

von Maltzahn, J., Jones, A.E., Parks, R.J., and Rudnicki, M.A. (2013). Pax7 is critical for the normal function of satellite cells in adult skeletal muscle. Proc. Natl. Acad. Sci. U S A *110*, 16474–16479.

Vousden, K.H., and Prives, C. (2009). Blinded by the light: the growing complexity of p53. Cell *137*, 413–431.

Wagers, A.J., and Conboy, I.M. (2005). Cellular and molecular signatures of muscle regeneration: current concepts and controversies in adult myogenesis. Cell *122*, 659–667.

Weintraub, H., Hauschka, S., and Tapscott, S.J. (1991). The MCK enhancer contains a p53 responsive element. Proc. Natl. Acad. Sci. U S A *88*, 4570–4571.

Westerberg, C.M., Hagglund, H., and Nilsson, G. (2012). Proteasome inhibition upregulates Bim and induces caspase-3-dependent apoptosis in human mast cells expressing the Kit D816V mutation. Cell Death Dis. *3*, e417.

Yin, H., Price, F., and Rudnicki, M.A. (2013). Satellite cells and the muscle stem cell niche. Physiol. Rev. *93*, 23–67.

Zeng, B.Y., Medhurst, A.D., Jackson, M., Rose, S., and Jenner, P. (2005). Proteasomal activity in brain differs between species and brain regions and changes with age. Mech. Ageing Dev. *126*, 760–766.

Supplemental Information

The Ubiquitin-Proteasome System Is Indispensable for the Maintenance of Muscle Stem Cells

Yasuo Kitajima, Naoki Suzuki, Aki Nunomiya, Shion Osana, Kiyoshi Yoshioka, Yoshitaka Tashiro, Ryosuke Takahashi, Yusuke Ono, Masashi Aoki, and Ryoichi Nagatomi
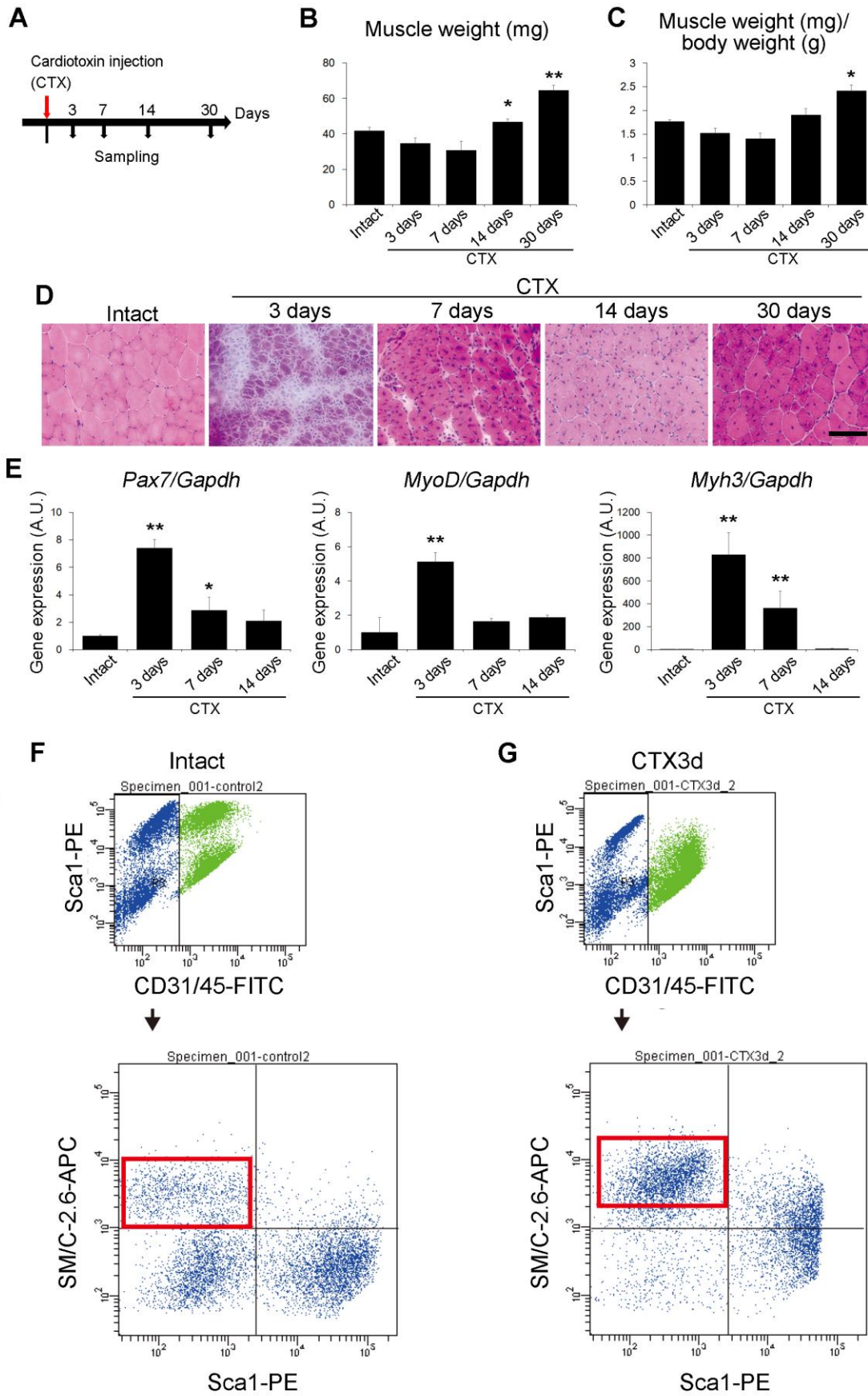
Figure S1. Histological and gene expression analysis during muscle regeneration. Related to Figure 1. (A) Time course for cardiotoxin (CTX) treatment and tissue harvesting. (B and C) Change in muscle weight (mg) and muscle weight (mg)/body weight (g). Data represent mean ± s.e.m. (t-test: *$P < 0.05$, **$P < 0.01$ vs intact (untreated) tissue, n = 5 per group). (D) HE staining of intact muscles and those injured by CTX injection analyzed at 3, 7, 14, and 30 days after injury. Scale Bar: 100 μm. Also shown in Figure 2F. (E) Real-time RT-PCR was used to measure the mRNA expression of myogenic regulatory factor genes (*Pax7* and *MyoD*) and *Myh3* in the tibialis anterior (TA) muscles at 3, 7, and 14 days after injury. Data represent means ± s.e.m. (t-test: *$P < 0.05$, **$P < 0.01$ vs intact; n = 3–5 per group). AU, arbitrary units. (F and G) FACS profiles of mononuclear cells derived from intact or injured muscles 3 days after cardiotoxin (CTX) injection. The red gated profiles show satellite cell fractions (SM/C-2.6+ CD31− CD45− Sca1−).
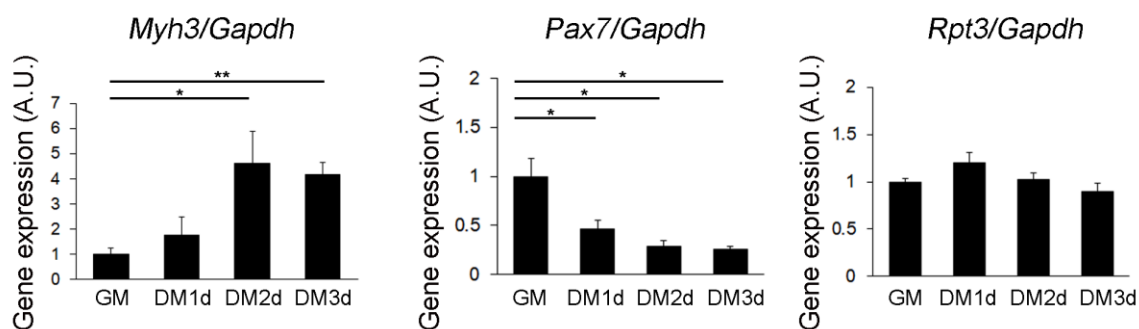
Figure S2

Figure S2. Relative expression of *Rpt3* mRNA in primary myoblasts during proliferation and differentiation process. Related to Figure 2. Relative expression of *Myh3*, *Pax7*, and *Rpt3* mRNA in primary myoblasts during proliferation and differentiation process. Data represent means ± s.d. (t-test: *$P < 0.05$, **$P < 0.01$; n = 3 per group). GM, growth medium. DM, differentiation medium. AU, arbitrary units.
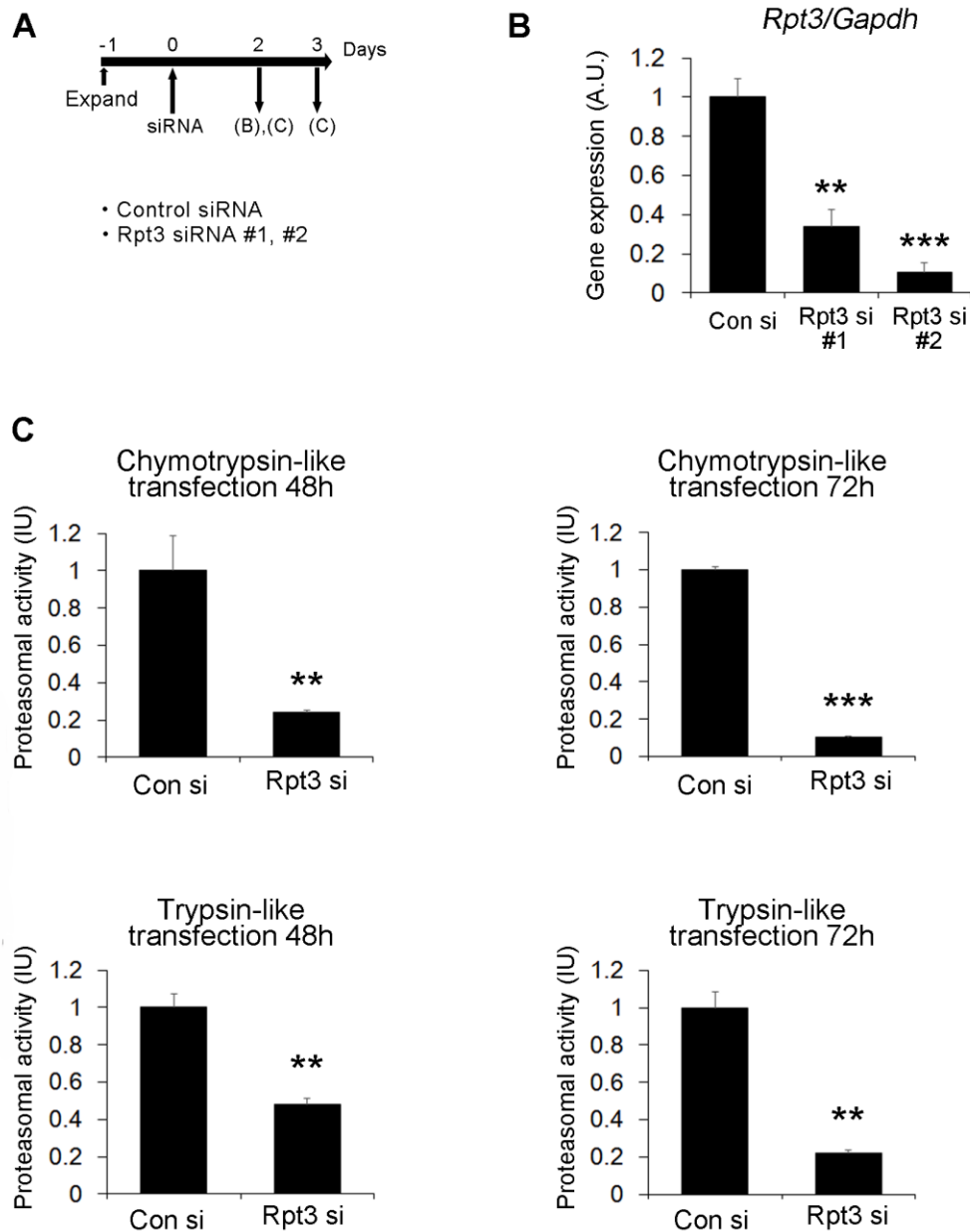
Figure S3. Inactivation of proteasome activity by *Rpt3* knockdown in C2C12 cell line. Related to Figure 2. (A) Time course of *Rpt3* siRNA knockdown in C2C12 cell line. (B) Relative expression of *Rpt3* and *Gapdh* mRNA in C2C12 cells after *Rpt3* siRNA transfection. Data represent means ± s.e.m. (t-test: **P < 0.01, ***P < 0.001; n = 3 per group). AU, arbitrary units. (C) Chymotrypsin-like and trypsin-like proteasome activities (relative to control siRNA) in C2C12 cell line. Data represent means ± s.e.m. (t-test: **P < 0.01, ***P < 0.001; n = 3 per group). IU, international units.
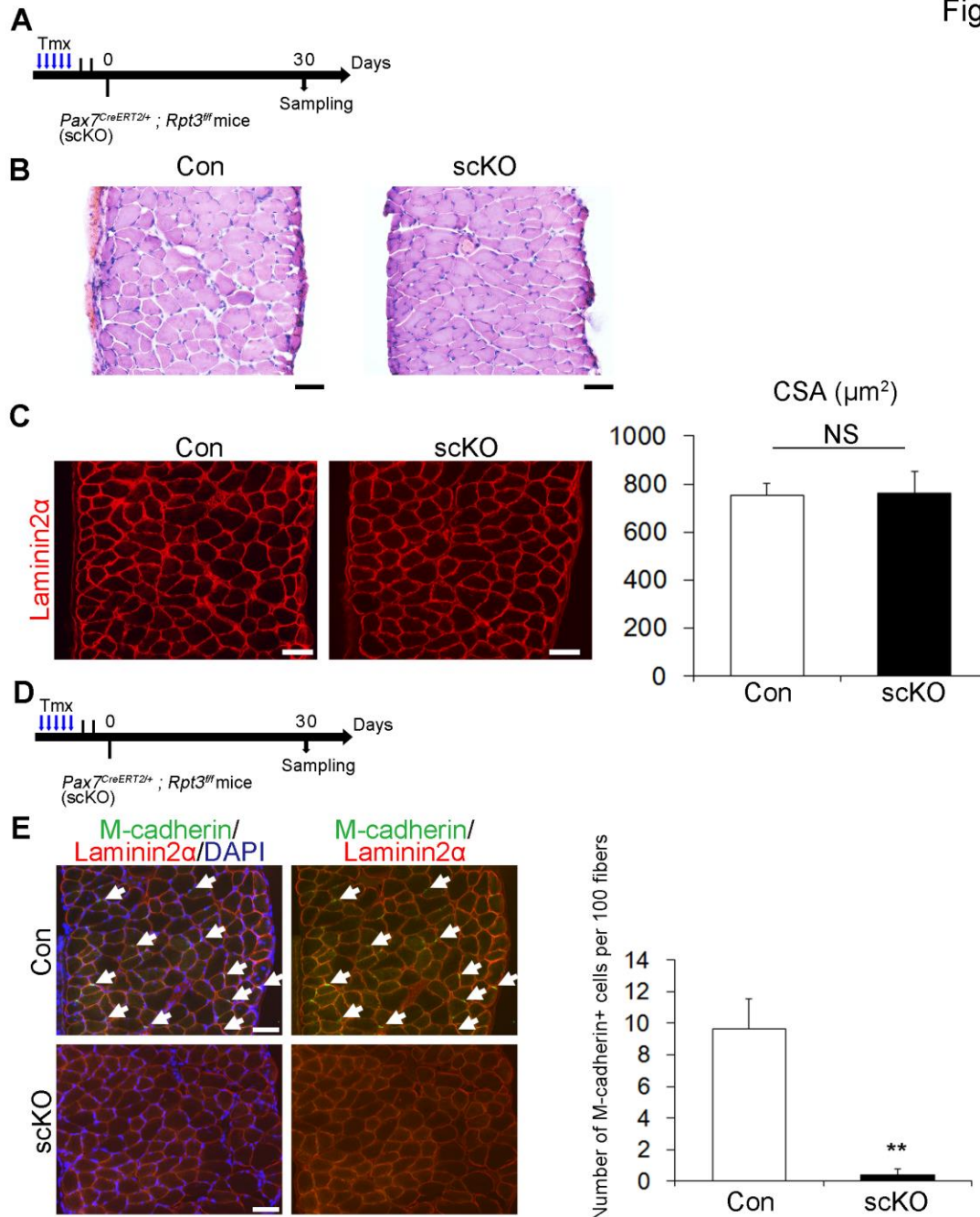
Figure S4. Histological analysis in diaphragm muscle 1 month after tmx treatment. Related to Figure 2 and Figure 4.

(A) Time course for tamoxifen (Tmx) treatment and tissue harvesting. Con indicates $Rpt3^{f/f}$ mice and scKO indicates satellite cell-specific $Rpt3$ knockout mice ($Pax7^{CreERT2/+}$; $Rpt3^{f/f}$). (B) HE staining of intact diaphragm muscles. Scale Bar: 50 μm. (C) Immunostaining for Laminin2α in intact diaphragm muscle cryosections from scKO mice. Scale Bar: 50 μm. The y-axis shows the mean cross-sectional area (CSA). Data represent means ± s.d. (t-test: NS, no significance; n = 4 per group). (D) Time course for Tmx treatment and tissue harvesting. (E) Immunostaining for M-cadherin (green), Laminin2α, and DAPI (blue) in intact diaphragm muscle cryosections from scKO mice. Arrows indicate satellite cells. Scale Bar: 50 μm. The y-axis shows average number of M-cadherin+ cells per 100 fibers. Data represent means ± s.d. (t-test: **P < 0.01; n = 3 per group).

A

Tmx ||||| || 0   15   Days

                 Sampling

B Con

Vcam1-APC

3.9%

CD31/45/Sca1-PE

C scKO

Vcam1-APC

0.9%

CD31/45/Sca1-PE

D

Relative MuSC fraction
(Vcam1+Sca-1−CD31−CD45−)

1.2
1
0.8
0.6
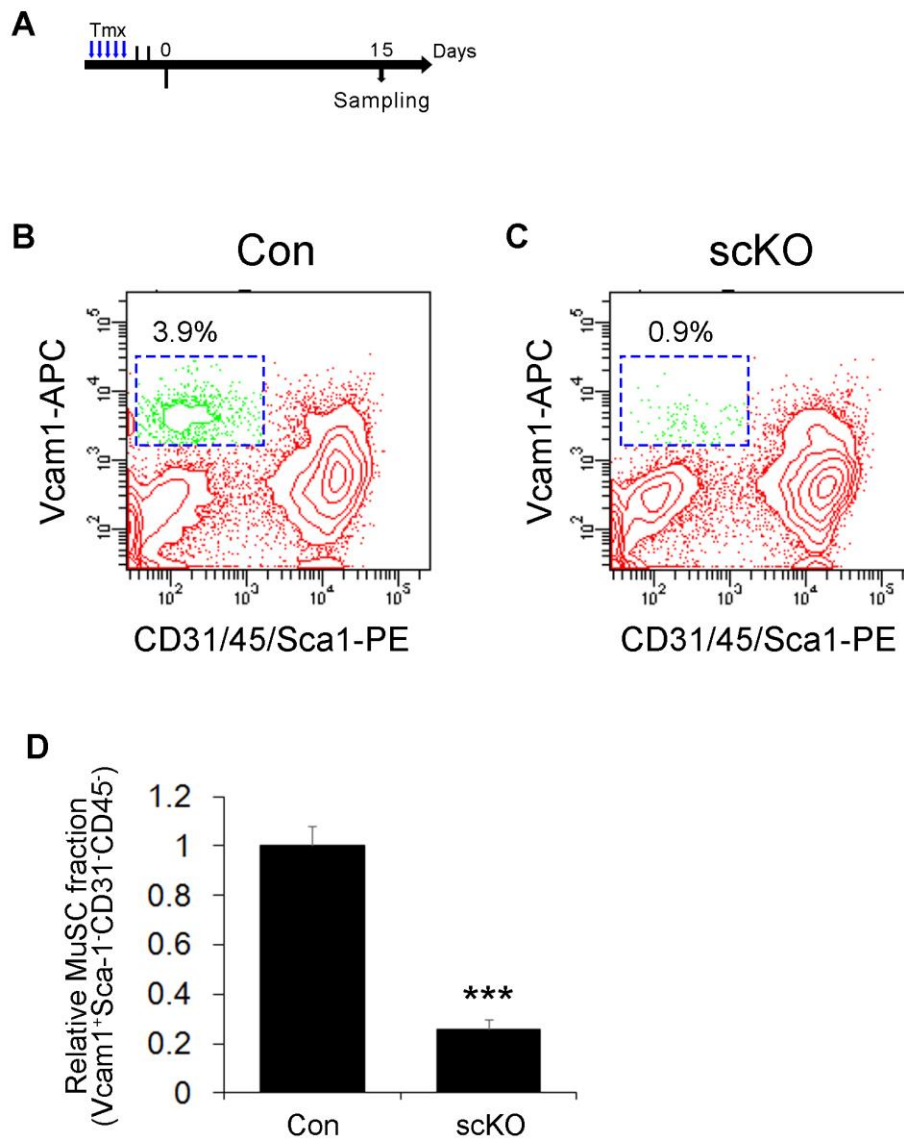0.4
0.2
0

***

Con   scKO

Figure S5. FACS profiles of mononuclear cells derived from scKO mice 15 days after Tmx treatment. Related to Figure 4. (A) Time analysis of tamoxifen (Tmx) treatment and tissue harvesting. Con indicates $Rpt3^{f/f}$ mice and scKO indicates satellite cell-specific $Rpt3$ knockout mice ($Pax7^{CreERT2/+}$; $Rpt3^{f/f}$). (B and C) FACS profiles of mononuclear cells derived from Con and scKO mice 15 days after Tmx treatment. The blue gated profiles show satellite cell fractions (Vcam1+ CD31− CD45− Sca1−) from Con and scKO mice. (D) Relative satellite cell fractions from Con and scKO mice. Data represent mean ± s.e.m. (t-test: *** P < 0.001; n = 3 for each group).
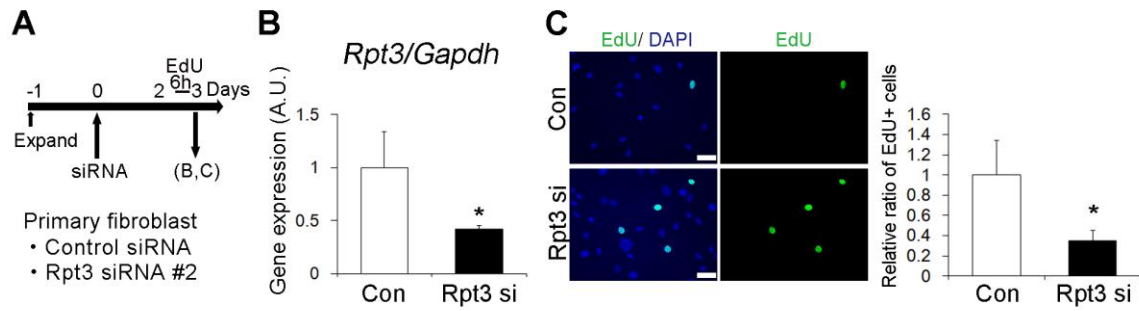
Figure S6. Proliferation defects in *Rpt3* knockdown of primary fibroblast. Related to Figure 6.

(A) Time course of *Rpt3* siRNA knockdown in primary fibroblast. (B) Relative expression of *Rpt3* and *Gapdh* mRNA in primary fibroblast after *Rpt3* siRNA transfection. Data represent means ± s.e.m. (t-test: *P < 0.05; n = 3 per group). AU, arbitrary units. (C) Immunostaining for EdU (green) and DAPI (blue) in primary fibroblast treated after *Rpt3* siRNA transfection. Scale bar: 50 μm. The y-axis shows the relative ratio of EdU-positive cells. Data represent means ± s.e.m. (t-test: *P < 0.05; n = 3 per group).
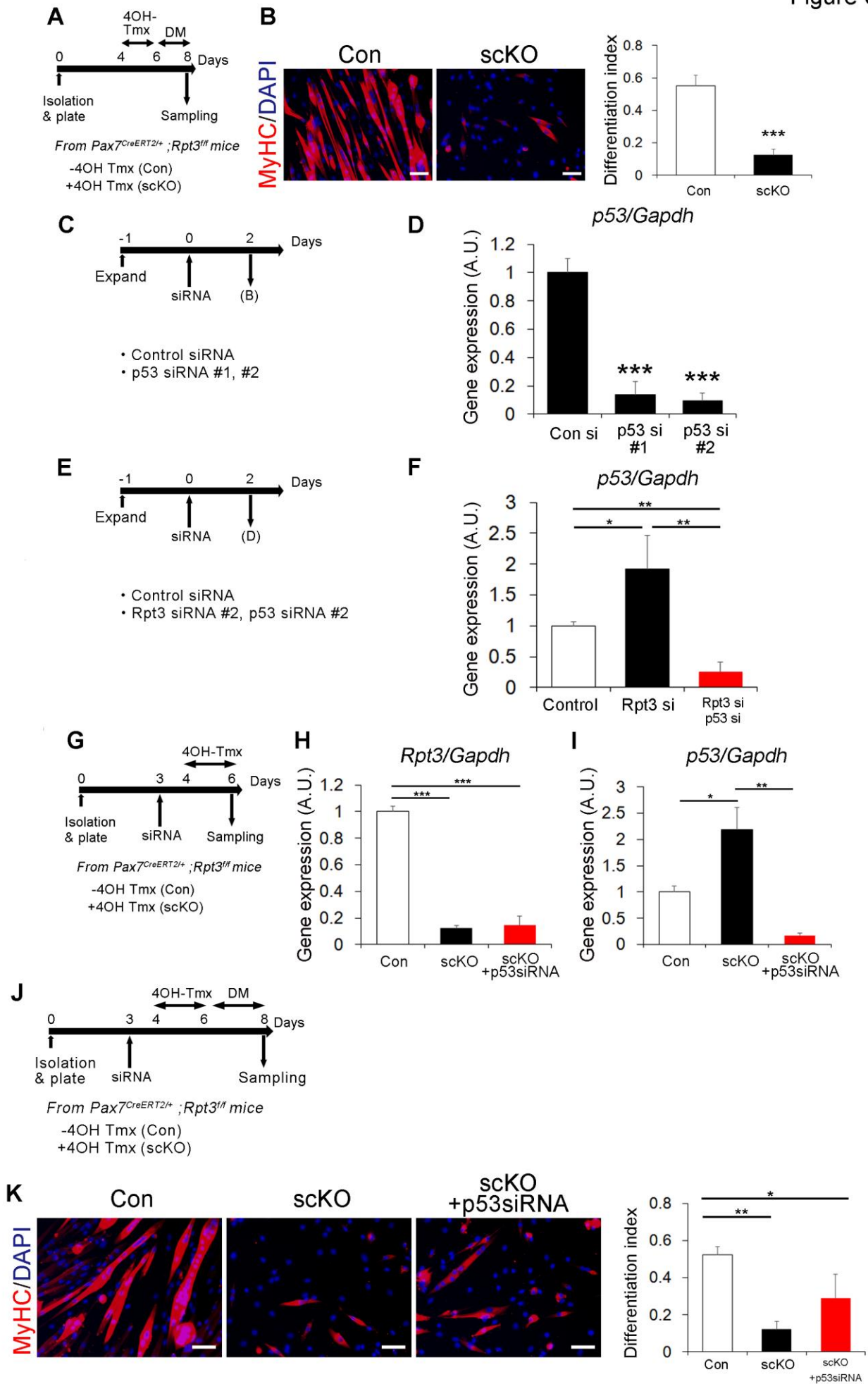
Figure S7

Figure S7. Deletion of Rpt3 in satellite cells induces differentiation defects. Related to Figure 6 and Figure 7.

(A) Time course analysis of tamoxifen (Tmx) treatment. (B) Myoblasts were induced to differentiate for 2 days and stained for MyHC (red); nuclei were counterstained with DAPI (blue). Scale bar: 50 μm. The differentiation index was calculated by dividing the number of nuclei in myotubes (MyHC-positive elongated cells) by the total number of nuclei. Data are shown as mean ± s.d. (t-test: ***P < 0.001; n = 4 per group). (C) Time course analysis of p53 siRNA knockdown in C2C12 cell line. (D) Relative expression of *p53* and *Gapdh* mRNA in C2C12 cells after p53 siRNA transfection. Data represent means ± s.e.m. (t-test: ***P < 0.001; n = 3 per group). AU, arbitrary units. (E) Time course analysis of *Rpt3* and *p53* siRNA knockdown in C2C12 cell line. (F) Relative expression of *p53* and *Gapdh* mRNA in C2C12 cells after *Rpt3* and *p53* siRNA transfection. Data represent means ± s.e.m. (one-way ANOVA followed by the Bonferroni post hoc test: * P < 0.05, ** P < 0.01; n = 4 per group). AU, arbitrary units. (G) Time course for analysis of *p53* siRNA knockdown and Tmx treatment. (H) Real-time RT-PCR was used to measure the mRNA expression of *Rpt3*. Data represent means ± s.e.m. (one-way ANOVA followed by the Bonferroni post hoc test: *** P < 0.001; n = 5-6 per group). AU, arbitrary units. (I) Real-time RT-PCR was used to measure the mRNA expression of *p53*. Data represent means ± s.e.m. (one-way ANOVA followed by the Bonferroni post hoc test: * P < 0.05, ** P < 0.01; n = 5-6 per group). AU, arbitrary units. (J) Time course analysis of *p53* siRNA knockdown and Tmx treatment. (K) Myoblasts were induced to differentiate for 2 days and stained for MyHC (red); nuclei were counterstained with DAPI (blue). Scale bar: 50 μm. The differentiation index was calculated by dividing the number of nuclei in myotubes (MyHC-positive elongated cells) by the total number of nuclei. Data are shown as mean ± s.d. (one-way ANOVA followed by the Bonferroni post hoc test: *P < 0.05, **P < 0.01; n = 3–5 per group).

Supplementary Table 1. Primers for quantitative RT-PCR. Related to Figure 2, Figure 6, Figure 7, and Figure S1, S2, S3, S6, S7.

Pax7-F	GTGCCCTCAGTGAGTTCGATTAGC	*Pax7-R*	CCACATCTGAGCCCTCATCCA
MyoD-F	AGCACTACAGTGGCGACTCA	*MyoD-R*	GCTCCACTATGCTGGACAGG
Rpt3-F	CTACAGGCCTTGCTCAGCTC	*Rpt3-R*	AGATTGTGGGCGTCTGTAGG
Gapdh-F	AACTTTGGCATTGTGGAAGG	*Gapdh-R*	CACATTGGGGGTAGGAACAC
Tbp-F	CAGATGTGCGTCAGGCGTTC	*Tbp-R*	TAGTGATGCTGGGCACTGCG
Myh3-F	GCCAGGATGGGAAAGTCACTGTGG	*Myh3-R*	GGGCTCGTTCAGGTGGGTCAGC
p53-F	ACGCTTCTCCGAAGACTGG	*p53-R*	AGGGAGCTCGAGGCTGATA
p21(Cdkn1a)-F	CGGTGTCAGAGTCTAGGGGA	*p21(Cdkn1a)-R*	AGGATTGGACATGGTGCCTG
Cyclind1(Ccnd1)-F	AGTGCGTGCAGAAGGAGATT	*Cyclind1(Ccnd1)-R*	CTCTTCGCACTTCTGCTCCT
Cdk4-F	GGCCCTCAAGAGTGTGAGAG	*Cdk4-R*	CATCAGCCGTACAACATTGG

Supplementary Table 2. Microarray analysis identified 1254 genes that were up- or down-regulated with p-values < 0.05 (satellite cells from satellite cell-specific *Rpt3* mice vs satellite cells from control mice). Related to Figure 7.

SUPPLEMENTAL EXPERIMENTAL PROCEDURES

Mouse strains

The Experimental Animal Care and Use Committee of Nagasaki University approved animal experimentation (Ref. No. 1203190970). Rpt3-floxed mice (Kitajima et al., 2014; Tashiro et al., 2012) were crossed with $Pax7^{CreERT2}$ mice (Lepper and Fan, 2010) to generate $Pax7^{CreERT2/+}$; $Rpt3^{f/f}$ (satellite cell-specific $Rpt3$ knockout) mice. All mice used for these experiments were between 2 and 3 months of age.

Mouse tissue preparation

The body and wet muscle were weighed. The TA muscles were collected individually using standard dissection methods and cleaned of excess fat, connective tissue, and tendons. The TA and diaphragm muscles were frozen in isopentane cooled with liquid nitrogen for histological and immunocytochemical analysis, and directly in liquid nitrogen for RNA isolation, and stored at -80 °C.

Mouse treatments

Tamoxifen (Tmx; Sigma) was dissolved in corn oil at a concentration of 20 mg/ml, and experimental and control mice were injected intraperitoneally with 150 μl (3mg) once per day for 5 days to induce Cre mediated excision.

Immunostaining

Immunocytochemistry of satellite cells and isolated single fibers was performed as described previously (Kitajima et al., 2016). Samples were incubated with primary antibodies at 4°C overnight following blocking/permeabilization with phosphate-buffered saline containing 0.3% triton X-100 and 5% goat serum for 20 min at RT. For immunohistochemistry, cryosections of muscle tissue were fixed with 4% PFA, blocked with 5 % goat serum or the M.O.M kit (Vector Laboratories) for 30 min at room temperature, and incubated with primary antibodies at 4 °C overnight. All immunostaining samples were visualized using appropriate species-specific Alexa Fluor 488 and/or 546 fluorescence-

conjugated secondary antibodies (Life Technologies). Samples were then observed using an Olympus fluorescence microscope IX83 (Olympus).

For EdU detection, the Click chemical reaction was performed after primary and secondary staining according to the manufacturer's instructions using a Click-iT EdU Imaging Kit (Life Technologies).

In vivo EdU-uptake assay

EdU was dissolved in PBS at 0.5 mg/ml and injected intraperitoneally at 0.1 mg per 20 g body weight at the time points indicated.

Immunoblotting

Total protein lysates were extracted from the mouse TA muscle and cultured satellite cells for immunoblotting analysis. We used the BCA method to determine protein concentrations. Then, the protein fractions were extracted with a reducing sample buffer containing 5% β-mercaptoethanol and complete protease inhibitor cocktail (Roche). The protein (20 µg per lane) samples were separated on a 10-20 % gradient SDS-polyacrylamide gels and subsequently transferred to polyvinylidene difluoride membranes (Millipore) at 250 mA for 1 h. The membrane was then incubated with primary antibodies. Specific signals were detected using the enhanced chemiluminescence method (GE Healthcare), as described previously (Kitajima et al., 2014). Densitometry was measured using ImageJ software (National Institute of Health).

Muscle injury

Cardiotoxin (CTX; Sigma-Aldrich) was prepared by dissolving a freshly opened tube in 0.9%NaCl at 10µM. Next, 50µl of CTX (10 µM) was injected percutaneously into the left TA muscles of anesthetized mice. Mice were allowed to recover for 3,7,14, or 30 days post-injury. Injected and contralateral TA muscles were harvested for sectioning and staining.

Preparation and FACS analyses of satellite cells

Mononuclear cells from uninjured limb muscles were prepared using 0.2% collagenase type II (Worthington Biochemical) as previously described (Kitajima et al., 2016). Mononuclear cells derived from skeletal muscle were stained with FITC-conjugated anti-CD31 (Biolegend, Cat. No. 102405), anti-CD45 (Biolegend, Cat. No. 103107), PE-conjugated anti-Sca-1 (Biolegend, Cat. No. 122507), and biotinylated anti-SM/C-2.6 (Fukada et al., 2004) antibodies. Cells were then incubated with streptavidin-APC (BD Biosciences, Cat. No. 554067) on ice for 30 min, and resuspended in PBS containing 2% FBS. Cell sorting was performed using a FACS Aria II flow cytometer (BD Immunocytometry Systems). Debris and dead cells were excluded by forward scatter, side scatter, and PI gating. Data were collected using FACS Diva software (BD Biosciences).

Proteasome activity

Proteasome activity was assessed using a Proteasome-Glo™ Assay kit (Promega), as we previously described (Gomes et al., 2001; Kitajima et al., 2014). The chymotrypsin-like and trypsin-like proteasome activities assays were conducted in a total volume of 100 μl in opaque 96-well plates. For the assays, protein contents from TA muscles or cells were added to assay buffer containing 20 mM Tris HCl (pH 7.2), 0.1 mM EDTA, 5 mM ATP, 1 mM β-mercaptoethanol, 20% glycerol and 0.04% Nonidet P40. The individual proteasome reagents were added separately, and the luminescence was recorded as relative light units on a Varioskan luminometer 30 min later (Thermo Scientific). Each sample was measured in duplicate or triplicate.

Real time PCR

Total RNA was isolated using RNeasy (Qiagen). For real-time PCR, first-strand cDNA was synthesized using oligo-dT primers. The expression levels of selected genes were analyzed using the Bio-Rad CFX96 system according to the manufacturer's instructions and quantitative PCR analysis was performed in triplicate using specific primers (Supplementary Table 1).

Gene expression microarrays

The cRNA was amplified, labeled, and hybridized to a 60K Agilent 60-mer oligomicroarray according to the manufacturer's instructions. All hybridized microarray slides were scanned by an Agilent scanner. Relative hybridization intensities and background hybridization values were calculated using Agilent Feature Extraction Software (9.5.1.1). Raw microarray data are available from the GEO public depository under the accession number: GEO: GSE114354.

Detection of apoptotic cells

For TUNEL staining, slides were fixed in 4% PFA for 10 min and then subjected to the TUNEL reaction using MEBSTAIN Apoptosis TUNEL Kit Direct (MBL), strictly following instructions provided by the manufacturer. Samples treated with DNaseI for 30 min before TUNEL staining was used as the positive control.

Antibodies

The following antibodies from Cell Signaling Technology were used: anti-GAPDH (Cat. No. 2118), phospho-p53 (Cat. No. 9281), p53 (Cat. No. 2524), Cyclin D3 (Cat. No. 2936), phospho-Rb (Cat. No. 9308), cleaved-caspase 3 (Cat. No. 9664), and M-cadherin (Cat. No. 40491). Antibodies against the following proteins were obtained from Biolegend: FITC-conjugated anti-CD31 (Cat. No. 102405), anti-CD45 (Cat. No. 102405), PE-conjugated anti-Sca-1 (Cat. No. 122507), and APC-conjugated anti-Vcam1 (Cat. No. 105718). Rpt3 (Cat. No. HPA002044) and laminin (Cat. No. L9393) were also from Sigma. The Pax7 (Cat. No. MAB1675) and MyHC (Cat. No. MAB4470) antibodies were purchased from R&D. We also used antibodies against MyoD (Cat. No. sc760) and eMyHC (Cat. No. sc53091) from Santa Cruz Biotechnology, ubiquitin (LifeSensors, Cat. No. VU101), and Collagen type I (Southern Biotech, Cat. No. 1310-01). Biotinylated anti-SM/C-2.6 antibody was a gift from Dr. Fukada (Fukada et al., 2004).

Running capacity assessment

The protocol of the maximal exercise test was performed as our described previously (Nunomiya et al., 2017). Briefly, before the test, the mice ran for 5 min at 10 m min^{-1} as a warm-up. During the first 30 min, the speed was set at 10 m min^{-1} and was increased by 2 m min^{-1} every 15 min. Throughout the warm-up and test running, the treadmill was set without slopes. Exhaustion was determined to be point at which the animal would not resume running for 15 s despite gentle brushing on the tail and a mild electrical foot shock.

Statistical analysis

Statistical analyses were performed with SPSS software (IBM) to determine significant differences based on a two-tailed distribution using a Student's t-test. For comparisons of more than two groups, a one-way analysis of variance (ANOVA) for repeated measures followed by the Bonferroni post hoc test was used. P values are indicated on each figure as < 0.05 (*), < 0.01 (**) and < 0.001 (***). All error bars represent means ± s.d. or s.e.m. NS represents statistically non-significant.

REFERENCES

Fukada, S., Higuchi, S., Segawa, M., Koda, K., Yamamoto, Y., Tsujikawa, K., Kohama, Y., Uezumi, A., Imamura, M., Miyagoe-Suzuki, Y., et al. (2004). Purification and cell-surface marker characterization of quiescent satellite cells from murine skeletal muscle by a novel monoclonal antibody. Exp Cell Res. *296*, 245-255.

Gomes, M.D., Lecker, S.H., Jagoe, R.T., Navon, A., and Goldberg, A.L. (2001). Atrogin-1, a muscle-specific F-box protein highly expressed during muscle atrophy. Proc Natl Acad Sci U S A. *98*, 14440-14445.

Kitajima, Y., Ogawa, S., and Ono, Y. (2016). Visualizing the Functional Heterogeneity of Muscle Stem Cells. Methods Mol Biol. *1516*, 183-193.

Kitajima, Y., Tashiro, Y., Suzuki, N., Warita, H., Kato, M., Tateyama, M., Ando, R., Izumi, R., Yamazaki, M., Abe, M., et al. (2014). Proteasome dysfunction induces muscle growth defects and protein aggregation. J Cell Sci. *127*, 5204-5217.

Lepper, C., and Fan, C.M. (2010). Inducible Lineage Tracing of Pax7-Descendant Cells Reveals Embryonic Origin of Adult Satellite Cells. Genesis. *48*, 424-436.

Nunomiya, A., Shin, J., Kitajima, Y., Dan, T., Miyata, T., and Nagatomi, R. (2017). Activation of the hypoxia-inducible factor pathway induced by prolyl hydroxylase domain 2 deficiency enhances the effect of running training in mice. Acta Physiol (Oxf). *220*, 99-112.

Tashiro, Y., Urushitani, M., Inoue, H., Koike, M., Uchiyama, Y., Komatsu, M., Tanaka, K., Yamazaki, M., Abe, M., Misawa, H., et al. (2012). Motor neuron-specific disruption of proteasomes, but not autophagy, replicates amyotrophic lateral sclerosis. J Biol Chem. *287*, 42984-42994.